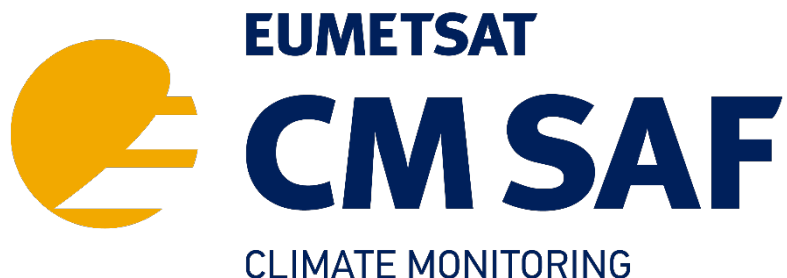


EUMETSAT Satellite Application Facility on Climate Monitoring



Validation Report

Microwave Imager Radiance FCDR Extension SSMIS Brightness Temperatures

DOI: [10.5676/EUM_SAF_CM/FCDR_MWI/V004](https://doi.org/10.5676/EUM_SAF_CM/FCDR_MWI/V004)

Microwave Imager Radiance FCDR R4.1

CM-12005

Reference Number:


SAF/CM/DWD/VAL/FCDR_MWI_CND

Issue/Revision Index:

1.0

Date:

2023-08-09

	Validation Report Microwave Imager Radiance FCDR R4.1 SSMIS Brightness Temperatures	Doc. No: SAF/CM/DWD/VAL/FCDR_MWI_CND Issue: 1.0 Date: 2023-08-09
---	--	--

Document Signature Table

	Name	Function	Signature	Date
Author	Karsten Fennig, Hannes Konrad	CM SAF Scientist		2023-08-09
Editor	Marc Schröder	Science Coordinator		2023-08-15
Approval	CM SAF Steering Group			
Release	Rainer Hollmann	Project Manager		


Distribution List

Internal Distribution	
Name	No. Copies
DWD / Archive	1
CM SAF Team	1

External Distribution		
Company	Name	No. Copies
PUBLIC		1

Document Change Record

Issue/ Revision	Date	DCN No.	Changed Pages/Paragraphs
1.0	2023-08-09	SAF/CM/DWD/VAL/FCDR_MWI_CND	DRR 4.11

	Validation Report Microwave Imager Radiance FCDR R4.1 SSMIS Brightness Temperatures	Doc. No: SAF/CM/DWD/VAL/FCDR_MWI_CND Issue: 1.0 Date: 2023-08-09
---	--	--

Applicable documents

Reference	Title	Code / Validity Date
AD 1	Memorandum of Understanding between CM SAF and the Max-Planck Institute for Meteorology and Meteorological Institute, University of Hamburg	1. March 2012
AD 2	CM SAF Product Requirements Document	SAF/CM/DWD/PRD/4.2

Reference documents

Reference	Title	Code
RD 1	Algorithm Theoretical Basis Document Fundamental Climate Data Record of SSMIS Brightness Temperatures	SAF/CM/DWD/ATBD/ FCDR_SSMIS/2.2
RD 2	Algorithm Theoretical Basis Document Fundamental Climate Data Record of SSM/I Brightness Temperatures	SAF/CM/DWD/ATBD/ FCDR_SSMI/2.2
RD 3	Product User Manual Fundamental Climate Data Record of SSM/I Brightness Temperatures	SAF/CM/DWD/PUM/ FCDR_SSMI/1.2
RD 4	Validation Report Fundamental Climate Data Record of SSM/I Brightness Temperatures	SAF/CM/DWD/VAL/ FCDR_SSMI/1.2
RD 5	Product User Manual Fundamental Climate Data Record of SSMIS Brightness Temperatures	SAF/CM/DWD/PUM/ FCDR_SSMIS/1.76
RD 6	Product User Manual Fundamental Climate Data Record of SMMR Brightness Temperatures	SAF/CM/DWD/PUM/ FCDR_SMMR/1.2
RD 7	Algorithm Theoretical Basis Document Fundamental Climate Data Record of SMMR Brightness Temperatures	SAF/CM/DWD/ATBD/ FCDR_SMMR/2.2
RD 8	Requirements Review Document Microwave Imager Radiance FCDR	SAF/CM/DWD/RR/3.1

Table of Contents

1	The EUMETSAT SAF on Climate Monitoring	6
2	Introduction	7
3	Validation of the SSMIS.....	9
3.1	Instrument and sensor stability.....	10
3.2	Inter-sensor evaluation of brightness temperature differences	14
3.2.1	Data sets for comparison	14
3.2.2	Evaluation strategy	15
3.2.3	Inter-Sensor Evaluation Results.....	17
3.3	Comparison against GMI	33
3.4	Evaluation of brightness temperature differences against reanalysis	38
3.5	Evaluation results	39
4	Conclusions.....	46
5	References.....	47
6	Glossary.....	49

List of Tables


Table 3-1: SSMIS FCDR instrument data availability at CM SAF.	9
Table 3-2: Requirement values for the SSMIS brightness temperatures product CM-12003 as given in the Product Requirements Document [AD 2].	15
Table 3-3: Statistics of the ensemble anomalies for SSMIS channel 19v GHz.....	20
Table 3-4: Statistics of instrument differences for SSMIS channel 19v GHz.	20
Table 3-5: Statistics of the ensemble anomalies for SSMIS channel 19h GHz.	22
Table 3-6: Statistics of instrument differences for SSMIS channel 19h GHz.....	22
Table 3-7: Statistics of the ensemble anomalies for SSMIS channel 22v GHz.....	24
Table 3-8: Statistics of instrument differences for SSMIS channel 22v GHz.	24
Table 3-9: Statistics of the ensemble anomalies for SSMIS channel 37v GHz.....	26
Table 3-10: Statistics of instrument differences for SSMIS channel 37v GHz.	26
Table 3-11: Statistics of the ensemble anomalies for SSMIS channel 37h GHz.....	28

Table 3-12: Statistics of instrument differences for SSMIS channel 37h GHz.....	28
Table 3-13: Statistics of the ensemble anomalies for SSMIS channel 91v GHz.....	30
Table 3-14: Statistics of instrument differences for SSMIS channel 91v GHz.....	30
Table 3-15: Statistics of the ensemble anomalies for SSMIS channel 91h GHz.....	32
Table 3-16: Statistics of instrument differences for SSMIS channel 91h GHz.....	32
Table 3-17: Estimated trends for global monthly mean differences between the simulated brightness temperatures from ERA5 and the combined inter-calibrated FCDR.....	39

List of Figures

Figure 3-1: Time series of DMSP platform mean local equator crossing times (top), altitude (middle) and Earth Incidence Angles (EIA) of the 91 GHz imager feedhorn (bottom) for all SSMIS instruments. Thin lines are the mean values at the ascending equator crossing and thick lines depict complete orbit mean values. Colours are as follows: F16 orange, F17 blue, F18 black.....	11
Figure 3-2: Time series of SSMIS sensor diagnostics: Temperature of the warm calibration target (upper panel) and temperature of the reflector arm (lower panel). The grey lines denote 0°C (for colours see Figure 3-1).	12
Figure 3-3: Time series of SSMIS sensor diagnostics: Radiometer sensitivities for the channels at 19v, 19h, 22v, 37v, 37h, 91v and 91h GHz. The grey lines denote the specification values.....	13
Figure 3-4: Time series of ensemble anomalies and variability for SSMIS channel 19v GHz. In the upper two panels the solid lines are PM orbits and the dashed lines AM orbits. The lower panels depict daily means of AM and PM orbits. The grey lines depict the ensemble spread. Horizontal grey lines denote the optimal and target bias. For a detailed description see text (section 3.2.2). Colours are as in Figure 3-1.	19
Figure 3-5: Same as Figure 3-4, but for SSMIS channel 19h GHz	21
Figure 3-6: Same as Figure 3-4, but for SSMIS channel 22v GHz.....	23
Figure 3-7: Same as Figure 3-4, but for SSM/I & SSMIS channel 37v GHz.....	25
Figure 3-8: Same as Figure 3-4, but for SSM/I & SSMIS channel 37h GHz.....	27
Figure 3-9: Same as Figure 3-4, but for SSMIS channel 91v GHz.....	29
Figure 3-10: Same as Figure 3-4, but for SSMIS channel 91h GHz.	31
Figure 3-11: Time series of global monthly mean anomalies of SSMIS minus GMI brightness temperatures at 22 GHz. The upper panel shows the homogenised data records and the lower panel depicts the inter-sensor calibrated SSMIS data record. Colours are as in Figure 3-1.	34
Figure 3-12: Time series of global monthly mean anomalies of SSMIS minus GMI brightness temperatures at 19 GHz. The upper two panels show the homogenised data records and the two lower panels depict the inter-sensor calibrated SSMIS data record. Colours are as in Figure 3-1.....	35

Figure 3-13: Time series of global monthly mean anomalies and SSMIS minus GMI channels at 37 GHz. The upper two panels show the homogenised data records and the two lower panels depict the inter-sensor calibrated SSMIS data record. Colours are as in Figure 3-1.	36
Figure 3-14: Time series of global monthly mean anomalies and SSMIS minus GMI channels at 91 GHz. The upper two panels show the homogenised data records and the two lower panels depict the inter-sensor calibrated SSMIS data record. Colours are as in Figure 3-1.	37
Figure 3-15: Time series of global monthly mean TB differences for the 19v GHz channel between the FCDR SSMIS instruments and ERA5. Colours for the instrument are F16 (orange), F17 (blue), F18 (black).....	40
Figure 3-16: Same as Figure 3-15 but for 19h GHz.	41
Figure 3-17: Same as Figure 3-15 but for 22v GHz.....	41
Figure 3-18: Same as Figure 3-15 but for 37v GHz.....	42
Figure 3-19: Same as Figure 3-15 but for 37h GHz.	42
Figure 3-20: Same as Figure 3-15 but for 85v GHz.....	43
Figure 3-21: Same as Figure 3-15 but for 85h GHz.	43
Figure 3-22: Same as Figure 3-15 but for 91v GHz.....	44
Figure 3-23: Same as Figure 3-15 but for 91h GHz.	44
Figure 3-24: Time series of robust standard deviation of global monthly mean TB differences for the channels 19v, 22v, 37v, and 85v GHz between the CM SAF FCDR and ERA5.	45

	Validation Report Microwave Imager Radiance FCDR R4.1 SSMIS Brightness Temperatures	Doc. No: SAF/CM/DWD/VAL/FCDR_MWI_CND Issue: 1.0 Date: 2023-08-09
---	--	--

1 The EUMETSAT SAF on Climate Monitoring

The EUMETSAT Satellite Application Facility on Climate Monitoring (CM SAF, <https://www.cmsaf.eu>), together with the EUMETSAT Secretariat, holds the role as main implementer of EUMETSAT's commitments in support to climate monitoring.


Since the beginning in 1999, CM SAF has developed and will continue to develop capabilities for a sustained generation and provision of Climate Data Records (CDR's) of Essential Climate Variables (ECVs) as defined by the Global Climate Observing System (GCOS), derived from operational meteorological satellites. In particular, the generation of long-term data records is pursued that are suitable for the analysis of climate variability and the detection of climate trends. Here, the main focus in CM SAF is on those ECVs that describe important components of the Earth's energy budget and its water cycle.

Another essential task of CM SAF is to produce data records that can serve applications related to the Global Framework of Climate Services initiated by the WMO World Climate Conference-3 in 2009. For this, CM SAF is supporting climate services at national meteorological and hydrological services with long-term data records but also with data sets produced in a seamless and coherent way close to real time that can be used to, e.g., prepare monthly/annual updates of the state of the climate. These so-called Interim Climate Data Records (ICDRs) together with the CDRs allow for a consistent description of mean values, anomalies, variability and potential trends for the considered ECVs. CM SAF CDRs also facilitate scientific applications such as for example process studies and evaluation of climate models at regional and global scales.

Furthermore, CM SAF contributes to advancing the availability, quality and usability of Fundamental Climate Data Records (FCDRs) in close collaboration with the EUMETSAT Secretariat and other satellite operators.

CM SAF is connected to the global scientific community ensuring a steady exchange of knowledge to continuously improve the data records and services, among others, through its engagement in international data assessments and through taking over responsibility in various international coordination bodies.

The international consortium of CM SAF currently comprises the Deutscher Wetterdienst (DWD) as host institute, the Royal Meteorological Institute of Belgium (RMIB), the Finnish Meteorological Institute (FMI), the Royal Meteorological Institute of the Netherlands (KNMI), the Swedish Meteorological and Hydrological Institute (SMHI), the Federal Office of Meteorology and Climatology (MeteoSwiss, Switzerland), the Meteorological Service of the United Kingdom (MetOffice, UK) and the Centre National de la Recherche Scientifique (CNRS, France).

	Validation Report Microwave Imager Radiance FCDR R4.1 SSMIS Brightness Temperatures	Doc. No: SAF/CM/DWD/VAL/FCDR_MWI_CND Issue: 1.0 Date: 2023-08-09
---	--	--

2 Introduction

This CM SAF validation report provides information on the evaluation of the Fundamental Climate Data Record (FCDR) of microwave brightness temperatures from the conical scanning microwave sensors Special Sensor Microwave/Imager (SSM/I), Special Sensor Microwave Imager/Sounder (SSMIS) and Scanning Multichannel Microwave Radiometer (SMMR). This fourth release is a continuation of the previous release (available from CM SAF; https://doi.org/10.5676/EUM_SAF_CM/FCDR_MWI/V003).


Data from the space-borne microwave imagers and sounders such as the Scanning Multichannel Microwave Radiometer (SMMR), Special Sensor Microwave/Imager (SSM/I) and the Special Sensor Microwave Imager/Sounder (SSMIS) are used for a variety of applications, such as analyses of the hydrological cycle (precipitation and evaporation) and related atmospheric and surface parameters, as well as remote sensing of sea ice, soil moisture, and land surface temperatures. Carefully calibrated and homogenised radiance data sets are a fundamental prerequisite for climate analysis, climate monitoring and reanalysis. Several National Meteorological Services and Reanalysis centres assimilate microwave radiances directly and not derived geophysical parameters. Forecast and reanalysis can thus benefit from a Fundamental Climate Data Record (FCDR) of brightness temperatures (Poli et al. 2015). The generation of Thematic Climate Data Records (TCDRs) strongly relies on the availability of FCDRs. Highest possible TCDR quality can be achieved easiest in radiance space, in turn increasing the products value for users.

The predecessors of this data record and the data processor suite have originally been developed at the Max-Planck Institute for Meteorology (MPI-M) and the University of Hamburg (UHH) for the Hamburg Ocean Atmosphere Parameters and Fluxes from Satellite Data (HOAPS, <http://www.hoaps.org/>) climatology. HOAPS is a compilation of climate data records for analysing the water cycle components over the global oceans derived from satellite observation (Andersson et al. 2011). The main satellite instrument employed to retrieve the geophysical parameters is the SSM/I and much work has been invested to process and carefully homogenize all SSM/I instruments onboard the Defence Meteorological Satellite Program (DMSP) platforms F08, F10, F11, F13, F14 and F15 (Andersson et al., 2010).

The HOAPS processing suite has been transferred to CM SAF in a Research to Operations activity in order to provide a sustained processing of the climate data records which is one of the main tasks of CM SAF, but not in the focus of the research group at the MPI-M / UHH. The operational processing and reprocessing of the FCDRs and TCDRs as well as the provision to the research community is maintained and coordinated by the CM SAF.

The first release of the CM SAF FCDR (Fennig et al. 2013) focussed on the SSM/I series, covering the time period from 1987 to end of 2008. This FCDR has already been used in the ESA CCI Sea ice project and in the reanalysis ERA5. In order to continue the HOAPS TCDRs beyond 2008 it was necessary to extend the underlying FCDR of microwave TBs with the SSMIS sensor family aboard the DMSP platforms F16, F17, and F18, which was accomplished with the second release of the CM SAF FCDR (Fennig et al. 2015). This combined FCDR of SSM/I and SSMIS brightness temperatures provides a consistent FCDR from 1987 to 2013.

Following requests from users of the FCDR, the third release focussed on the extension of the microwave brightness temperature data record to the earlier time period from 1978 to 1987

	Validation Report Microwave Imager Radiance FCDR R4.1 SSMIS Brightness Temperatures	Doc. No: SAF/CM/DWD/VAL/FCDR_MWI_CND Issue: 1.0 Date: 2023-08-09
---	--	--

with observations from the SMMR on-board Nimbus-7. However, this turned out to be a very challenging task, as it has not been possible to get hold of the original raw instrument data records. Although this data record must have eventually been transferred from the Marshall Space Flight Centre (MSFC) to the National Snow & Ice Data Center (NSIDC), it is currently not available from their archives. Instead, the Nimbus-7 SMMR Pathfinder Level 1B Brightness Temperatures data record, available from NSIDC (Njoku, 2003), is used to generate this FCDR.

With the fourth release of the Microwave Imager Radiance FCDR, the temporal coverage of the SSMIS had been extended to 31 December 2020 while the SMMR and SSM/I data records remain unchanged. The data records for the SSMIS sensors on-board F16, F17, and F18 have been reprocessed for this fourth FCDR release, implementing significant improvements. The same algorithm and processing tools are used for R4 of SSM/I and SMMR data as for the predecessor CM-12002. A detailed list of changes for this release is available in the corresponding ATBD for the SSMIS component [RD 1].

Responding to a user request, the SSMIS part of the Microwave Imager Radiance FCDR is extended with data from 2021 and 2022 with the release R4.1. The inter-calibration coefficients and the technical specifications remain unchanged compared to the fourth release and the SSMIS ATDB [RD 1] is still applicable. This validation report focuses on the of the SSMIS part of the FCDR, with an emphasis on the two extension years.

3 Validation of the SSMIS

The CM SAF FCDR from SSMIS brightness temperatures is compiled as daily collections of all observations from each sensor. All sensor specific data available in the raw data records are provided as well as additional information like quality control flags, Earth incidence angles (EIA), averaged 91 GHz brightness temperatures, synthetic 85 GHz brightness temperatures, incidence angle normalisation offsets, solar calibration correction offsets, and inter-sensor calibration offsets. The new SSMIS FCDR is now available for the time period from November 2005 until December 2022. A detailed list of data availability for each of the three SSMIS platforms is given in Table 3-1.

A technical description of the data set, including information on the file format as well as on the data access is provided in the corresponding Product User Manual [RD 5]. More details on the CM SAF inter-sensor calibration model, the implementation of the processing chain and individual processing steps are described in the SSMIS Algorithm Theoretical Basis Document [RD 1]. Basic accuracy requirements are defined in the product requirements document [AD 2]. An extensive description of the SSMIS instrument and satellite characteristics can be found in Kunkee et al. (2008).

Table 3-1: SSMIS FCDR instrument data availability at CM SAF.

DMSP platform	Launch date	Record start	Record end
F16	2003-10-18	2005-11-01	2022-12-31
F17	2006-11-04	2006-12-14	2022-12-31
F18	2009-10-18	2010-03-08	2022-12-31

3.1 Instrument and sensor stability

Figure 3-1 shows the time series of the mean DMSP platform local equator crossing times, altitude and the Earth Incidence Angles (EIA) of the 91 GHz feedhorn for the different SSMIS instruments. The local overpass time is changing for all platforms. The strongest drift can be observed for DMSP F16 and F18 from 8 to 4 AM/PM, while DMSP F17 depict a more constant equator crossing time around 6 AM/PM. Due to this drift in the local overpass time, the brightness temperature (TB) differences between the instruments are not constant and the diurnal cycle variation must be considered during the inter-sensor calibration and when comparing the inter sensor differences.

The altitude of the satellite platforms remains very constant over time, as depicted in the Figure 3-1, middle panel. Due to varying alignments of the imager feedhorn on the different platforms, the mean EIA ranges between 52.9 to 53.3 degrees (Figure 3-1, lower panel). The mean orbit EIA remains constant for SSMIS_{F16} and SSMIS_{F17}. The mean EIA of SSMIS_{F18} increases in May 2011 due to a change in the platform pitch angle. The SSMIS_{F18} depicted an artificial trend in the v-pol channels, as documented in the validation report of the FCDR release R2 (Fennig et al., 2015). The most likely scenario explaining this feature is a change in the attitude pitch angle. Though undocumented in the available literature but corrected for also by CSU, the pitch angle was changed in the processing software from FCDR release R3 onwards to remove the observed bias.

There are no noticeable anomalies visible for the years 2021-2022 in the altitude or mean EIA.

The regular seasonal variation of the local EIA at equator crossing (thin lines in Figure 3-1 lower panel), is caused by the orbit precession and can also lead to differences up to 0.2 degree in EIA. Since a change of 0.1 degree in EIA will change the vertical polarized TB up to 0.2 K, these variations must be considered by normalizing the observed TBs to a constant EIA. The CM SAF FCDR data files contain offsets, which are computed using the Furhop and Simmer (1996) algorithm to normalize the TBs to constant EIA of 53 degree. This TB offset can be applied if the user's application is designed for constant zenith angles and is only valid over ocean.

Figure 3-2 shows the time series of hot load target temperatures and reflector arm temperatures for all three SSMIS instruments. The temperature of the warm calibration target remains very constant at about 310 K. Only two short events can be observed in 2018 for the SSMIS_{F18}, where the mean warm target temperature drops to 290 K. This is a clear improvement over the SSM/I design, where a strong seasonal variability reaching an amplitude of up to 50 K was observed (see also the SSM/I validation report [RD 4]). The variation in the reflector arm temperature is an important indicator for the correction of the SSMIS reflector emissivity problem. The temperature depends on the amount of time spent in the Earth shadow during an orbit and thus on the local equator overpass time. This dependency can be observed from the change in the seasonal arm temperature variations of SSMIS_{F16} and SSMIS_{F18}, when the overpass time drifts from 8 to 4 AM/PM. In the beginning the seasonal variation in the warm target temperature is very small, but starts to undergo strong cooling events from 2011 (2017) onward, when the local overpass time has drifted before 7 AM/PM. The minima in the arm temperatures are occurring at solar equinox in spring and autumn. When SSMIS_{F17} and SSMIS_{F16} are at the same overpass time in 2012, the seasonal arm temperature variations are

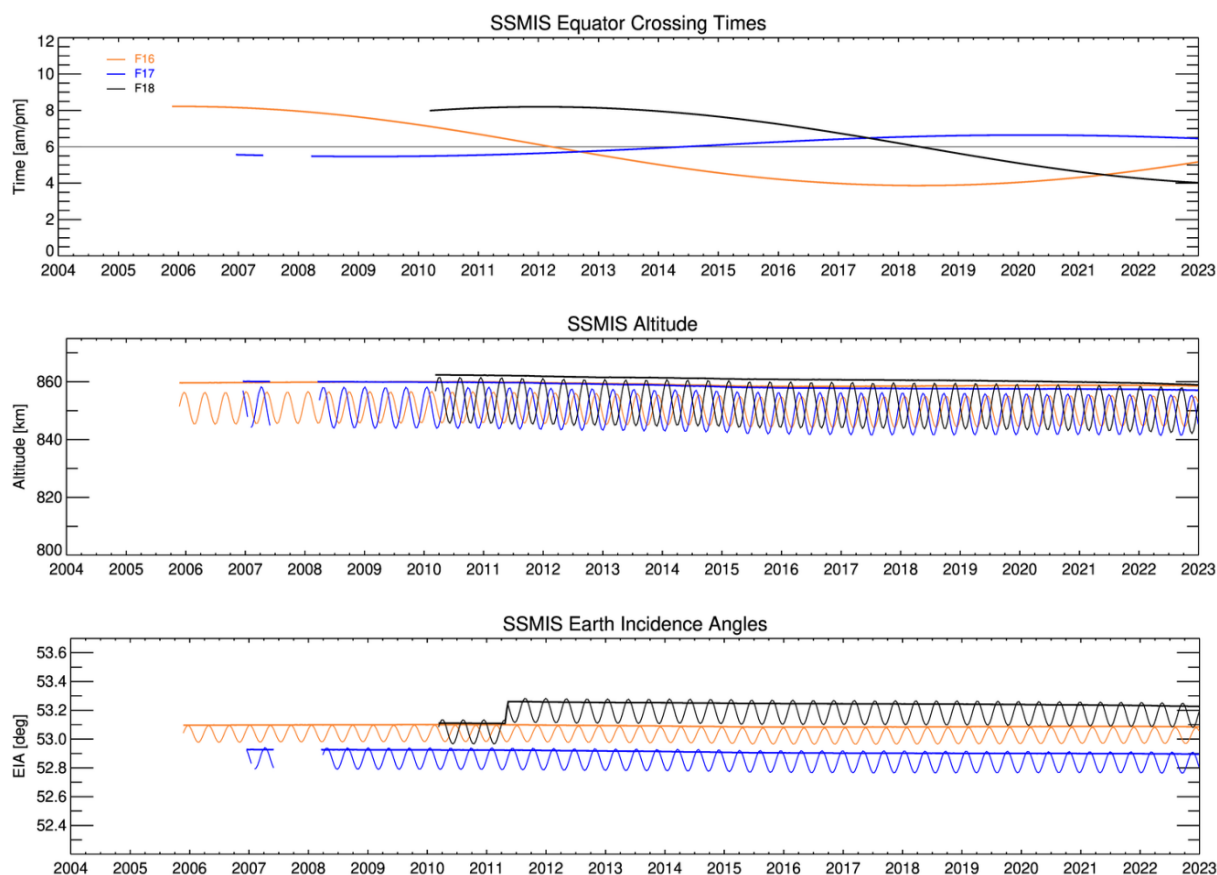


Figure 3-1: Time series of DMSP platform mean local equator crossing times (top), altitude (middle) and Earth Incidence Angles (EIA) of the 91 GHz imager feedhorn (bottom) for all SSMIS instruments. Thin lines are the mean values at the ascending equator crossing and thick lines depict complete orbit mean values. Colours are as follows: F16 orange, F17 blue, F18 black.

nearly identical. This can also be observed for SSMIS_{F17} and SSMIS_{F18} in 2017/2018. In 2014 the SSMIS_{F16} cooling events fade away, when the local overpass time is before 5 AM/PM.

A very strong decrease of the arm temperature can be observed for SSMIS_{F16} from 2016 onwards. The mean SSMIS_{F16} arm temperature drops to 190 K at the end of 2020. This trend continues throughout 2021 and 2022, reaching a temperature of 175 K at the end of 2022. As the SSMIS_{F16} has an emissive reflector, this strong trend would be detectable in the uncorrected TBs. However, after applying the emissivity correction, an artificial trend in the TBs at 91 GHz was observed, leading to the conclusion that the temperature sensor of the SSMIS_{F16} reflector operates erroneously since 2016. The SSMIS emissivity correction procedure was modified to account for this issue (see the SSMIS ATBD for more details [RD 1]). However, this correction has an impact on the quality of the TBs after 2016.

Figure 3-3 shows the time series of the radiometer sensitivities for all SSM/I-like channels. The radiometer noise equivalent differential temperature ($NEdT$) is estimated at the warm calibration target temperature (see the corresponding ATBD [RD 1]) and is available as a daily mean value from the CM SAF FCDR data files for all SSMIS channels. Overall, the radiometer noise is within the specification for most of the channels. The most pronounced feature of the SSMIS_{F18} is a sharp increase in the noise level in early 2012, visible in all channels. The maximum impact can be observed in the 37h channel, showing an increase from 0.4 K to

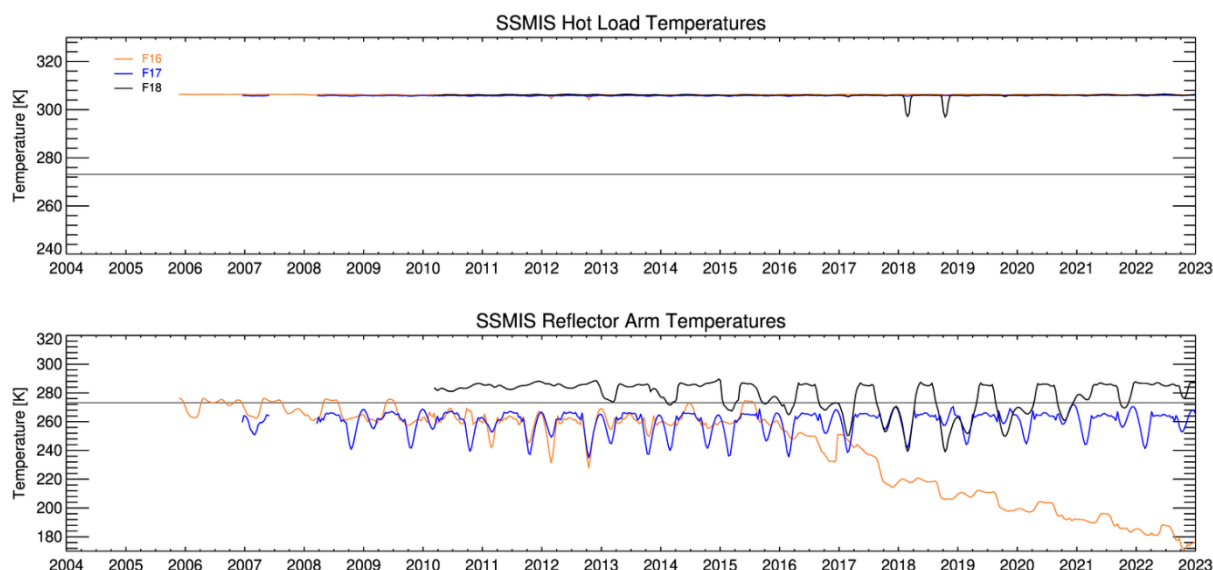


Figure 3-2: Time series of SSMIS sensor diagnostics: Temperature of the warm calibration target (upper panel) and temperature of the reflector arm (lower panel). The grey lines denote 0°C (for colours see Figure 3-1).

0.8 K. Also, an overall increase in the noise level in 2015, 2020 and 2021/2022 can be detected for SSMIS_{F18}. Again, the 37h channel is affected most, reaching the design specification at the end of 2015 and exceeding the specification in 2020 and again between March 2021 and March 2022. All SSMIS_{F17} channels behave inconspicuously. However, the 22v channel shows a slight upward trend but remains within the specification. Both 91 GHz channels of the SSMIS_{F16} are affected by a strong anomaly in summer 2015. The most problematic channel is the 91h channel of the SSMIS on-board F16. It is above the specification for most of the time and depicts a very noisy behaviour. The *NEdT* stays within the specification noise level only in 2014, 2017 and during June 2021 and June 2022.

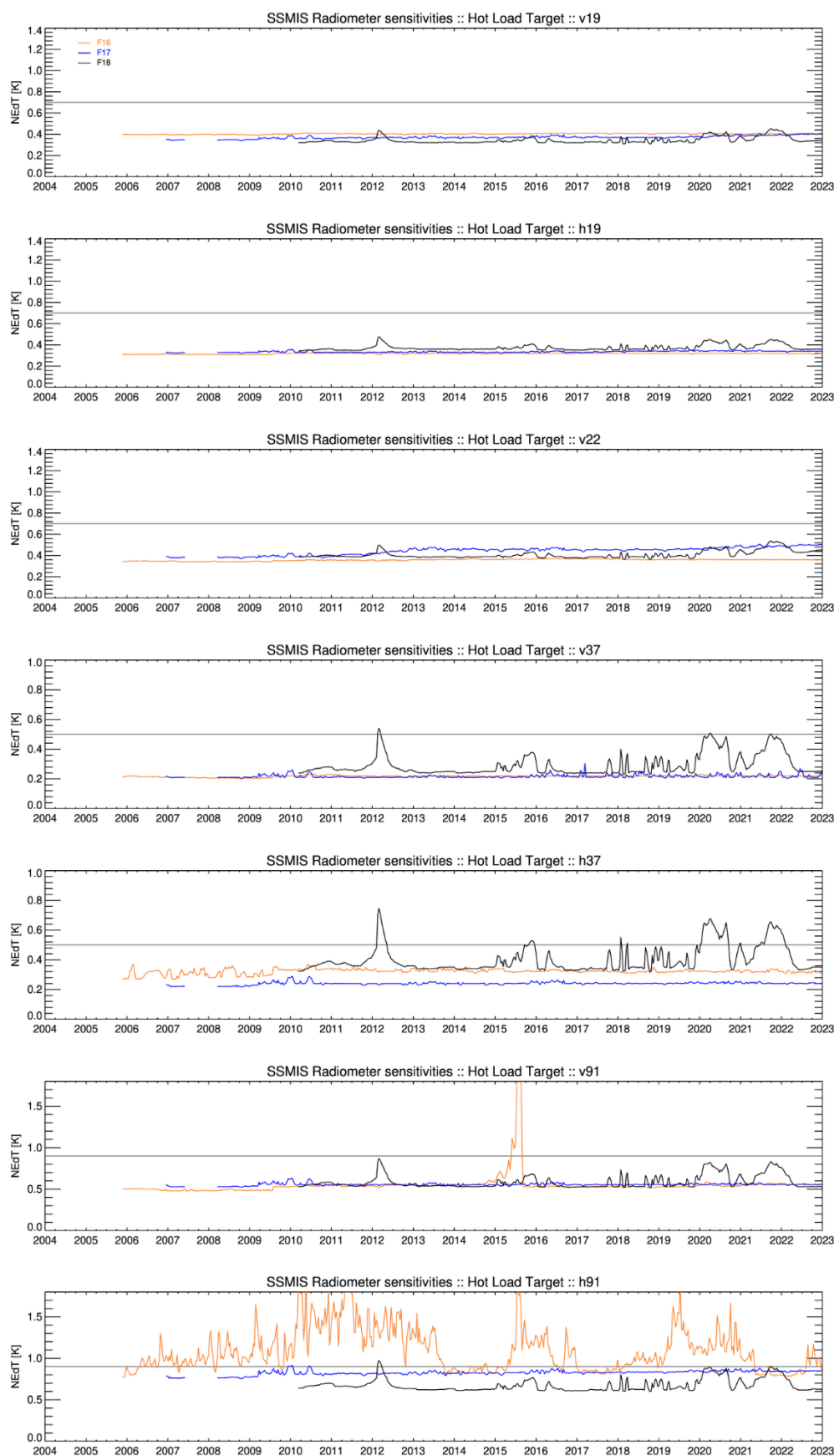



Figure 3-3: Time series of SSMIS sensor diagnostics: Radiometer sensitivities for the channels at 19v, 19h, 22v, 37v, 37h, 91v and 91h GHz. The grey lines denote the specification values.

	Validation Report Microwave Imager Radiance FCDR R4.1 SSMIS Brightness Temperatures	Doc. No: SAF/CM/DWD/VAL/FCDR_MWI_CND Issue: 1.0 Date: 2023-08-09
---	--	--

3.2 Inter-sensor evaluation of brightness temperature differences

The purpose of a validation is to establish, that the measurement under scrutiny agrees with an independent, and (ideally) traceable, measurement or estimate, within the combined measurement uncertainties in both. A conclusion from the error budget estimation (see ATBD [RD 1]) is, that a complete comprehensive validation of the SMMR / SSM/I / SSMIS brightness temperatures is not possible, as there is no absolute validation reference available. The final aim of an evaluation process must be to show that the measured brightness temperatures are in agreement with modelled brightness temperatures within the expected random uncertainties. As a major requisite, a Fundamental Climate Data Record must show improved quality compared to the existing Raw Data Records (RDR) in order to be a useful data set, providing added value to the user community.

Hence, the main validation strategy in this document is to compare this FCDR of SSMIS brightness temperatures to the original RDR and to another data record (CSU SSMIS FCDR (Berg, 2013)), in order to quantify the quality of the inter-sensor calibration and to compare the different inter-sensor calibration approaches. The aim of this validation report is to show that the homogeneity of the reprocessed FCDR is significantly improved compared to the original raw Temperature Data Records.

In addition to this inter-sensor comparison, a comparison of SSMIS observation against GMI brightness temperatures is presented in section 3.3. Finally, also a comparison against modelled brightness temperatures, using the ERA5 reanalysis data set, is conducted in section 3.4 in order to analyse the stability of the final FCDR across the platforms.

3.2.1 Data sets for comparison

Another FCDR of SSMIS brightness temperature has been released from Colorado State University (CSU). The inter-sensor calibration model used for this data set is described in detail in Sapiano and Berg (2013) and Berg and Sapiano (2012). The CSU inter-calibration model uses the SSM/I_{F13} as reference instrument. The inter-calibration is implemented in a two-step process. First a matchup database against rain-free TMI observation over ocean is used to correct for solar intrusion effects. This data base consists of double differences (SSMIS-model)-(TMI-model) as a function of solar azimuth, solar elevation, and scene temperature. After this correction to TMI has been applied, the SSMIS TBs are inter-calibrated to the SSM/I_{F13} using the mean of different types of double differences. The scene dependence is solved via a look-up table with fixed tie-points. For TBs outside the covered range, the maximum and minimum values are applied respectively.

A new version of the CSU FCDR has been released in 2022 (Kummerow et al., 2022). The main difference compared to the CSU FCDR version 1 is a change of the calibration reference from SSM/I_{F13} to the GMI. However, only relative differences between the SSMIS instruments of each FCDR are analysed in the next section. Therefore, the absolute calibration reference is not relevant in this context. Hence the new CSU FCDR version 2 is analysed for the extension period of 2021/2022, while for the time period from 2005-2020 the old CSU FCDR results are presented.

3.2.2 Evaluation strategy

The CM SAF FCDR is compared to the RDR and the CSU brightness temperature data record. The homogeneity of the data sets is tested by comparing against the respective ensemble mean of the available satellites in each data record and additional statistical values are given for bias, robust standard deviation (RSD), median absolute deviation (MAD) and decadal stability. The requirements for the SSMIS brightness temperature product are defined in the Product Requirements Document (PRD) [AD 2]. Table 3-2 recalls these requirements for monthly global mean values.


In order to quantify the consistency of the brightness temperatures across the SSMIS sensors, a reference has to be established first. As there is no absolute reference available and the operating sensors change over time, we choose the ensemble mean of all available instruments at each month as the relative reference. This approach simplifies the further analysis, as it can be performed per sensor and not for all sensor pairs. The inter-sensor differences are derived by comparing the respective bias values to the ensemble mean. The maximum inter-sensor difference is the ensemble spread, which characterizes the observation uncertainty, because without additional information each sensor could be treated as the “true” observation.

A global monthly mean bias only characterizes the mean systematic offset to another sensor. However, it is also important to quantify the observed regional differences, which is characterized by the distribution of gridded monthly mean brightness temperature differences. The median of absolute differences (MAD), without correcting for the mean systematic offset (bias), is a measure of the total absolute uncertainty. In terms of monthly mean gridded data samples, a MAD of 1 K means that 50% of all grid box brightness temperature differences are within 0-1 K. A robust (resilient to outliers) measure of the statistical dispersion of a distribution is the median absolute deviation about the median. Assuming a normal distribution, the expected standard deviation can be estimated from the median absolute deviation by scaling it with a factor of 1.48. For comparison, this approach has also been applied to the CSU data set which covers the same time period as the CM SAF FCDR. Prior to consistency analysis, the data files have first been converted to the CM SAF data format. Then both data sets have been gridded to equal angle 1° monthly mean global fields separately for AM and PM orbits. For the comparisons all oceanic grid cells are used.

To evaluate the relative instrument differences, an ensemble mean data set has been compiled for each FCDR on a monthly basis for all instruments and channels. The ensemble monthly mean grid box brightness temperature $\langle T_B \rangle$ for each month t and grid box index g is calculated

Table 3-2: Requirement values for the SSMIS brightness temperatures product CM-12003 as given in the Product Requirements Document [AD 2].

	Threshold	Target	Optimal
Bias	3 K	2 K	1 K
Decadal stability $t_D = 0.03$ K/decade	Significance $\alpha \geq 0.3\%$	Significance $\alpha \geq 5\%$	Significance $\alpha \geq 30\%$

	Validation Report Microwave Imager Radiance FCDR R4.1 SSMIS Brightness Temperatures	Doc. No: SAF/CM/DWD/VAL/FCDR_MWI_CND Issue: 1.0 Date: 2023-08-09
---	--	--

as the arithmetic mean of the individually gridded monthly mean brightness temperatures T_B from all available instruments s :

$$\langle T_B \rangle(t, g) = \frac{1}{N_s} \cdot \sum_{s=1}^{N_s} T_B(s, t, g), \quad \text{Equation 1}$$

with N_s as the number of contributing instruments for each grid box and month.

The distribution of brightness temperature differences ΔT_B relative to this ensemble mean

$$\Delta T_B(s, t, g) = T_B(s, t, g) - \langle T_B \rangle(t, g) \quad \text{Equation 2}$$

is then statistically analysed. Here, we apply robust statistics (see above), with M as the median of the distribution of all grid box brightness temperature differences ΔT_B for each instrument s . We define:

$$\begin{aligned} Bias_s &= M(\Delta T_B(t, g)|_s) \\ MAD_s &= M(|\Delta T_B(t, g)|_s) \\ RSD_s &= M(|Bias_s - \Delta T_B(t, g)|_s) \cdot 1.48 \end{aligned} \quad \text{Equation 3}$$

The requirement for the global monthly mean consistency between the instruments is given in Table 3-2 in terms of inter-sensor biases. As $Bias_s$ is relative to the ensemble mean, the inter-sensor bias is derived as the corresponding difference $Bias_{s1} - Bias_{s2}$.

The decadal stability t_D for each channel and instrument is estimated using a linear model trend, fitted to the time series of monthly anomalies relative to the ensemble mean. The anomalies are defined as the median of the global distribution of brightness temperature differences ΔT_B :


$$\overline{\Delta T_{B,s}}(t) = M[\Delta T_B(g)|_s](t). \quad \text{Equation 4}$$

A simple model with a linear decadal trend t_D in K/decade is then defined as:

$$\overline{\Delta T_{B,s}}(t) = \overline{\Delta T_{B,s}}(t = 0) + \frac{t_D}{120} \cdot t + \varepsilon(t), \quad \text{Equation 5}$$

with $\varepsilon(t)$ representing the fraction of the monthly anomalies not explained by the linear approximation. The linear model terms (offset and trend) are found by a least square regression fit. The stability requirement, as defined in the requirement review (Table 3-2, RD 8, AD 2), is a decadal stability with a linear trend of $t_D < 0.03 \text{ K/decade}$. The requirement levels are defined in terms of significance levels of statistical hypothesis testing. The null hypothesis $t_D > 0.03 \text{ K/decade}$ can be rejected (criterion is met), if the probability of rejecting the null hypothesis is higher than the threshold (0.3%), target (5%) or optimal (30%) criterion (see Table 3-2). The significance level α of the decadal trend is determined using a two-sided t-test, applying a standard uncertainty of 0.1 K from the distribution of the global monthly anomalies.

The results of the statistical analysis are shown in Figure 3-4 to Figure 3-10 and summarized in Table 3-3 to Table 3-16, grouped by channel. The tables also contain the maximum inter-sensor bias, which is the maximum absolute bias difference, computed using the first equation

	Validation Report Microwave Imager Radiance FCDR R4.1 SSMIS Brightness Temperatures	Doc. No: SAF/CM/DWD/VAL/FCDR_MWI_CND Issue: 1.0 Date: 2023-08-09
---	--	--

in Equation 3. All figure panels contain five images with time series of global monthly mean values of:

1. TB anomalies of the raw data record without any modification,
2. TB anomalies after reflector emissivity correction, EIA normalization, and diurnal cycle removed,
3. TB anomalies of the CM SAF FCDR
inter-sensor calibration offsets and solar calibration correction offsets applied,
4. TB anomalies of the CSU FCDR,
5. Robust standard deviation (RSD) of CM SAF FCDR TB anomalies.

3.2.3 Inter-Sensor Evaluation Results

The time series of the raw data records plots (RDR, Figure 3-4 to Figure 3-10 top panel) show a very diverse picture. Most of the SSMIS channels (19v, 19h, 22v, 37v) are in good agreement after the homogenisation step with remaining differences of up to 0.2 K. The differences are larger for 37h with about 1 K and reach a maximum of 2 K for the 91 GHz channels.

The calibration enhancement due to intrusion and reflector emissivity corrections (from first to second panel) and the inter-calibration (from second to third panel) reduce the inter-sensor variations and increase the quality and stability of the SSMIS data record significantly. The final global climatological mean inter-satellite bias of the SSMIS has been reduced to below 0.05 K.

Further results are summarised as follows:

- Both analysed FCDRs (CM SAF, CSU) significantly reduce the observed differences between the monthly means and show very similar results for individual satellites. All global monthly mean inter-sensor differences are within the optimum requirement of 1 K. In terms of maximum inter-sensor bias (ensemble spread), the CM SAF FCDR is performing slightly better. Comparing the absolute maximum difference between the individual satellite biases to the ensemble mean, the CM SAF FCDR shows a remaining ensemble spread of 0.03 K, while for the CSU FCDR values up to 0.19 K remain.
- Clearly visible is the version change of the CSU FCDR after December 2020. The agreement between the instruments is better in version 1 as compared to version 2 for most channels. The SSMIS_{F17} data is not available in both CSU FCDR versions after summer 2016.
- Overall, the monthly anomalies show a variability which is larger for horizontally polarized channels and increases with higher frequencies. This variability is caused by the inclusion of all scenes, i.e. no rain filtering is applied. This additional noise can be interpreted as an additional uncertainty due to differences in space and time collocation and sampling variability.
- No significant trend above the target criteria can be detected. SSMIS_{F18} channels 37h and 91h show a trend of -0.18 K/dec and -0.16 K/dec and the SSMIS_{F17} channel 91h depicts a trend of +0.14 K/dec. These trends are most pronounced in the last years of the covered time period. This is most likely related to limitations of the applied solar

correction. The parameters of this correction have been fitted for the time period until 2020. Applying this correction for a time period with solar angles beyond the fitted range can result in an underestimation of the solar effects. The solar correction is performing better in the other channels of the SSMIS_{F18}, where the trend, visible in the uncorrected data, is effectively removed.

- A periodic increase in the TB bias is visible in the CSU FCDR for most channels from early 2015 onwards. The ensemble spreads depict maximum offsets of about 0.5K in northern hemispheric winter. This feature is also visible in the homogenised data records (second panel). This instrument related issue is removed in the CM SAF FCDR. It can also be noted that this variation is smaller in the new CSU FCDR version.
- A significant anomaly above 1 K difference is found in summer 2015 in the 91 GHz channels of F16. This also corresponds to an observed increase in *NEdT* during this time period as described in section 3.1 (compare also Figure 3-3). Another smaller anomaly of about 1 K is visible in winter 2014 in the 91v channel. Both deviations are smaller in the CM SAF FCDR compared to the CSU FCDR.
- The robust standard deviations depict constant values over time for all channels and instruments between 0.5 K and 1 K. This means, that about 70% of all analysed monthly mean grid boxes are within ± 0.5 K to ± 1 K, respectively. The outliers above 1 K are caused by incomplete months and therefore increased variability due to a shorter sampling period.
- The statistical measures derived from both FCDRs depict a very good and similar performance of both data sets in terms of RSD and MAD. However, some channels (22v, 19h) in the CSU FCDR show a small remaining bias of about 0.2 K.
- The noise level of all instruments is very similar.
- The large seasonal variations of the TB differences at 91 GHz (first panels) are caused by the reflector emissivity issue, affecting the instruments on-board SSMIS_{F16} and SSMIS_{F17}. These anomalies are in the order of 1 K for the global mean and larger in the horizontal polarised channels. These anomalies are corrected for in the CM SAF FCDR and only small variations remain in the homogenised plots (second panels).

Overall it can be concluded that the extension period continues the FCDR homogeneously. However, as the solar correction remains fixed, the observed variability is not removed completely for all channels and global mean differences of about 0.2 K remain for some channels.

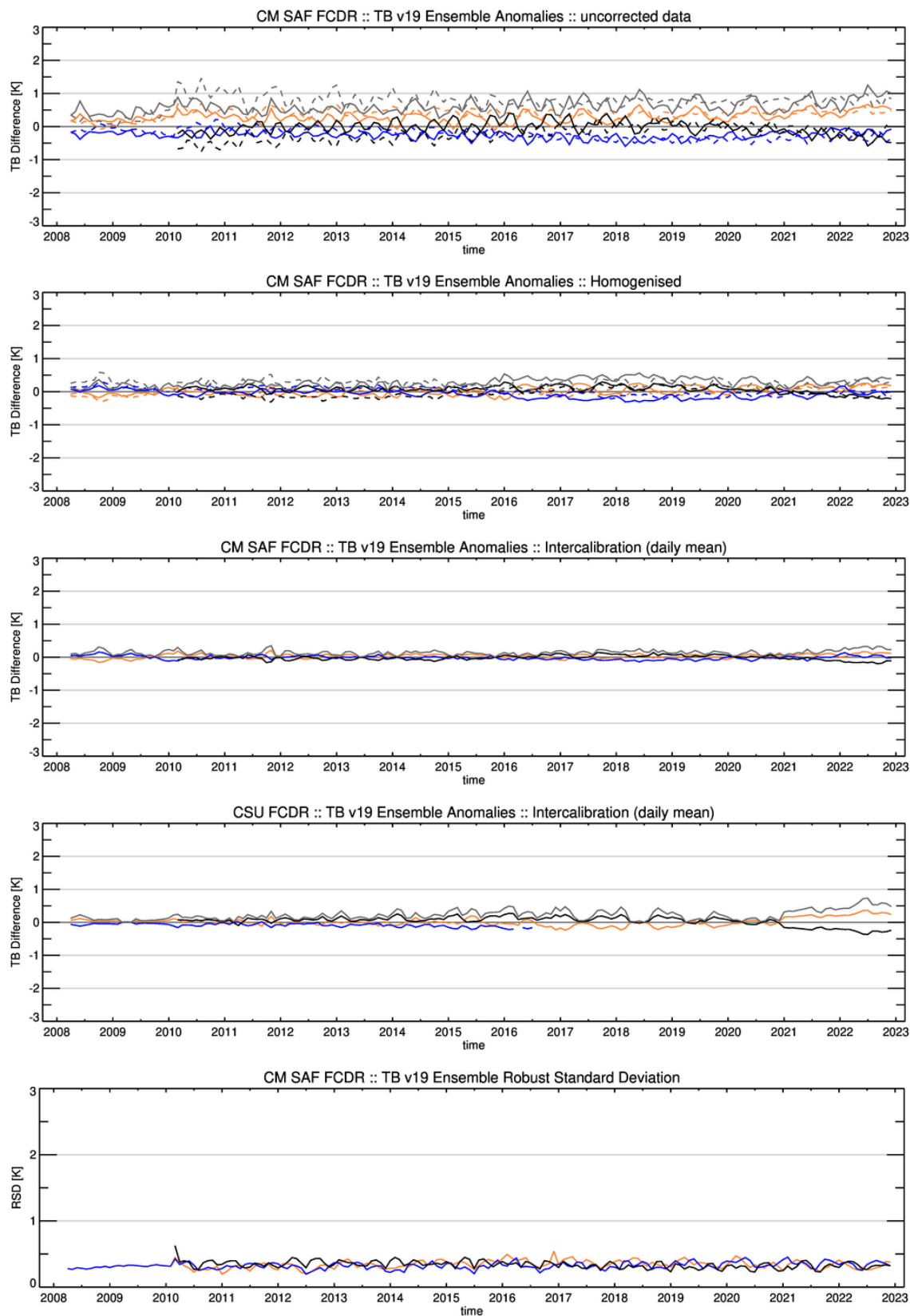


Figure 3-4: Time series of ensemble anomalies and variability for SSMIS channel 19v GHz. In the upper two panels the solid lines are PM orbits and the dashed lines AM orbits. The lower panels depict daily means of AM and PM orbits. The grey lines depict the ensemble spread. Horizontal grey lines denote the optimal and target bias. For a detailed description see text (section 3.2.2). Colours are as in Figure 3-1.


	Validation Report Microwave Imager Radiance FCDR R4.1 SSMIS Brightness Temperatures	Doc. No: SAF/CM/DWD/VAL/FCDR_MWI_CND Issue: 1.0 Date: 2023-08-09
---	--	--

Table 3-3: Statistics of the ensemble anomalies for SSMIS channel 19v GHz. The first block shows the original RDR with EIA normalized, the second block the CM SAF FCDR and the last block the CSU FCDR.

	F16	F17	F18
Bias [K]	0.00	-0.02	+0.02
RSD [K]	0.35	0.35	0.36
MAD [K]	0.24	0.24	0.25
max absolute inter-sensor Bias [K]	0.01	0.06	0.06
Bias [K]	0.03	-0.01	-0.01
RSD [K]	0.34	0.33	0.35
MAD [K]	0.24	0.23	0.23
max absolute inter-sensor Bias [K]	0.06	0.04	0.06
Trend [K/dec]	0.07 ($\alpha > 30\%$)	-0.05 ($\alpha > 30\%$)	0.02 ($\alpha > 30\%$)
Bias [K]	0.02	-0.08	0.04
RSD [K]	0.35	0.33	0.38
MAD [K]	0.24	0.24	0.26
max absolute inter-sensor Bias [K]	0.09	0.19	0.19

Table 3-4: Statistics of instrument differences for SSMIS channel 19v GHz. The numbers represent percentiles of absolute differences less than 1K, 2K, and 3K of all individual monthly mean grid boxes between two instruments.

	F16	F17	F18
F16		84.2 97.2 99.4	84.2 97.3 99.5
F17			85.2 97.5 99.5

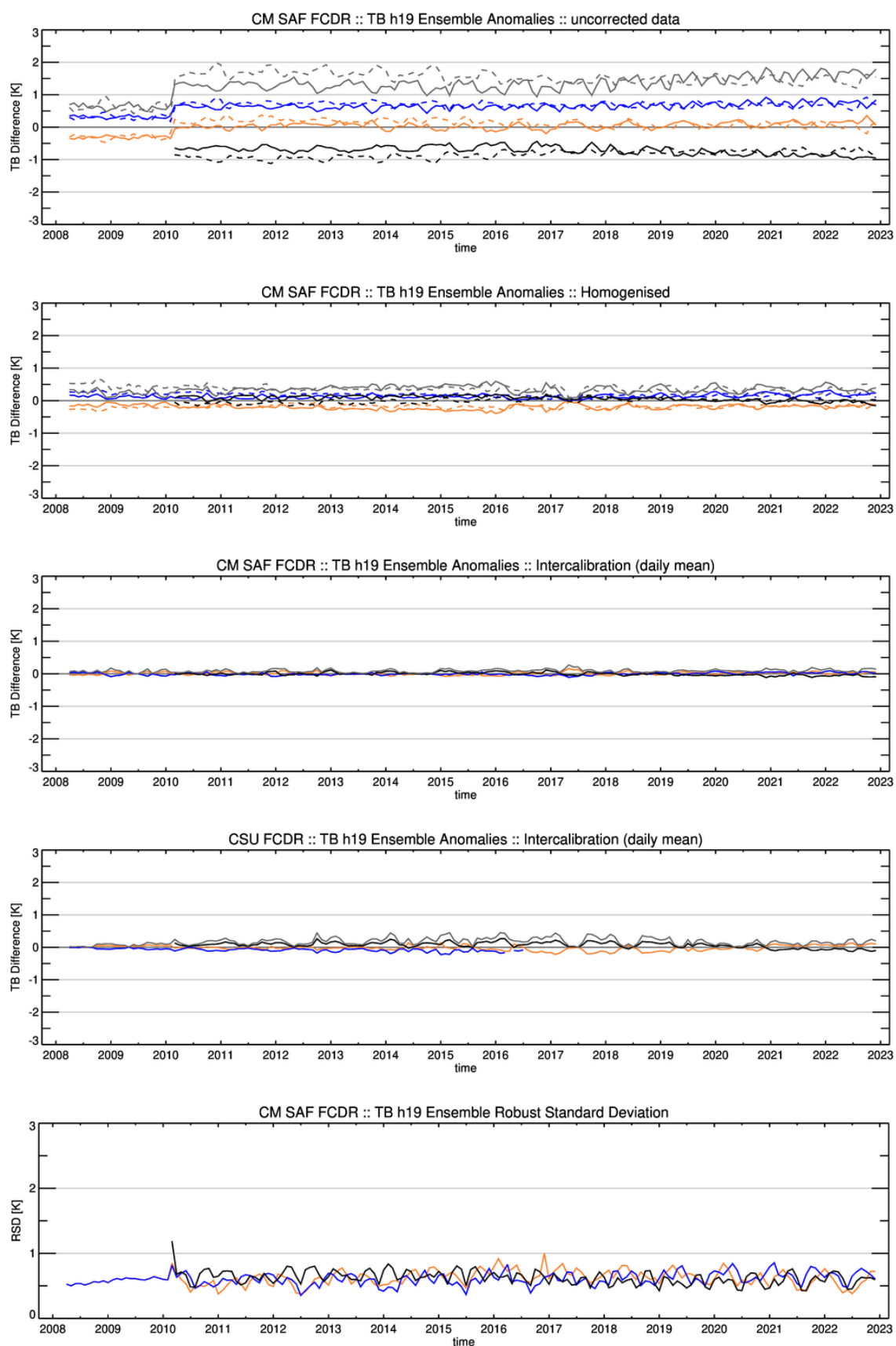


Figure 3-5: Same as Figure 3-4, but for SSMIS channel 19h GHz


	Validation Report Microwave Imager Radiance FCDR R4.1 SSMIS Brightness Temperatures	Doc. No: SAF/CM/DWD/VAL/FCDR_MWI_CND Issue: 1.0 Date: 2023-08-09
---	--	--

Table 3-5: Statistics of the ensemble anomalies for SSMIS channel 19h GHz. The first block shows the original RDR with EIA normalized, the second block the CM SAF FCDR and the last block the CSU FCDR.

	F16	F17	F18
Bias [K]	-0.19	+0.16	+0.03
RSD [K]	0.61	0.61	0.62
MAD [K]	0.44	0.43	0.42
max absolute inter-sensor Bias [K]	0.35	0.35	0.21
Bias [K]	+0.01	-0.01	-0.01
RSD [K]	0.62	0.61	0.62
MAD [K]	0.42	0.41	0.42
max absolute inter-sensor Bias [K]	0.02	0.01	0.02
Trend [K/dec]	+0.02 ($\alpha > 30\%$)	+0.04 ($\alpha > 30\%$)	-0.05 ($\alpha > 30\%$)
Bias [K]	-0.02	-0.08	+0.06
RSD [K]	0.57	0.59	0.60
MAD [K]	0.38	0.41	0.41
max absolute inter-sensor Bias [K]	0.08	0.20	0.20

Table 3-6: Statistics of instrument differences for SSMIS channel 19h GHz. The numbers represent percentiles of absolute differences less than 1K, 2K, and 3K of all individual monthly mean grid boxes between two instruments.

	F16	F17	F18
F16		62.8 86.7 94.9	62.9 87.0 95.1
F17			63.7 87.6 95.4

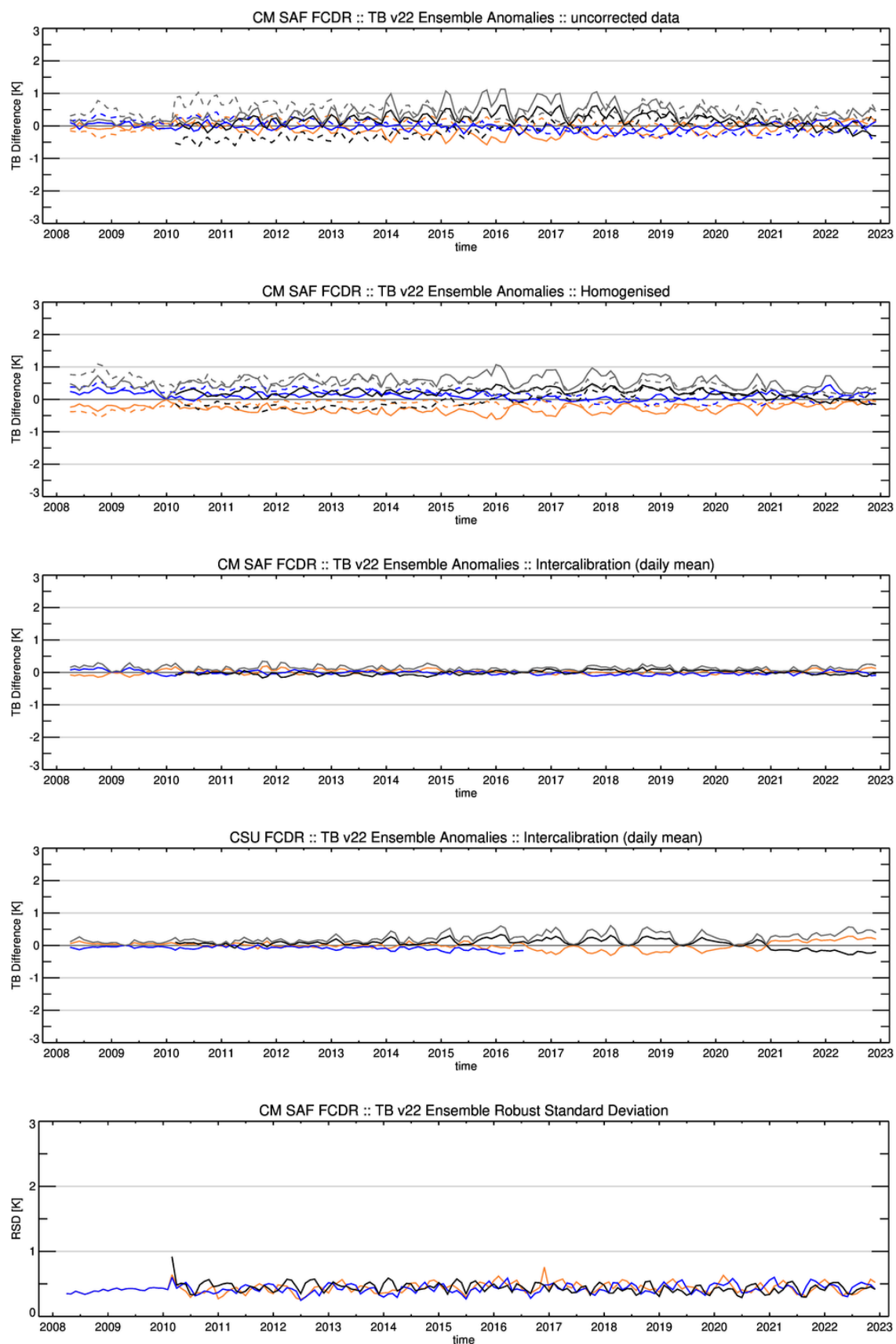


Figure 3-6: Same as Figure 3-4, but for SSMIS channel 22v GHz.


	Validation Report Microwave Imager Radiance FCDR R4.1 SSMIS Brightness Temperatures	Doc. No: SAF/CM/DWD/VAL/FCDR_MWI_CND Issue: 1.0 Date: 2023-08-09
---	--	--

Table 3-7: Statistics of the ensemble anomalies for SSMIS channel 22v GHz. The first block shows the original RDR with EIA normalized, the second block the CM SAF FCDR and the last block the CSU FCDR.

	F16	F17	F18
Bias [K]	-0.23	+0.15	+0.10
RSD [K]	0.46	0.46	0.47
MAD [K]	0.36	0.34	0.33
max absolute inter-sensor Bias [K]	0.38	0.38	0.32
Bias [K]	+0.02	-0.01	-0.01
RSD [K]	0.44	0.43	0.44
MAD [K]	0.30	0.30	0.30
max absolute inter-sensor Bias [K]	0.03	0.03	0.01
Trend [K/dec]	+0.02 ($\alpha > 30\%$)	-0.05 ($\alpha > 30\%$)	+0.08 ($\alpha > 30\%$)
Bias [K]	-0.00	-0.08	+0.06
RSD [K]	0.43	0.43	0.46
MAD [K]	0.29	0.30	0.31
max absolute inter-sensor Bias [K]	0.09	0.19	0.19

Table 3-8: Statistics of instrument differences for SSMIS channel 22v GHz. The numbers represent percentiles of absolute differences less than 1K, 2K, and 3K of all individual monthly mean grid boxes between two instruments.

	F16	F17	F18
F16		76.4 94.2 98.3	76.6 94.6 98.5
F17			77.5 94.9 98.6

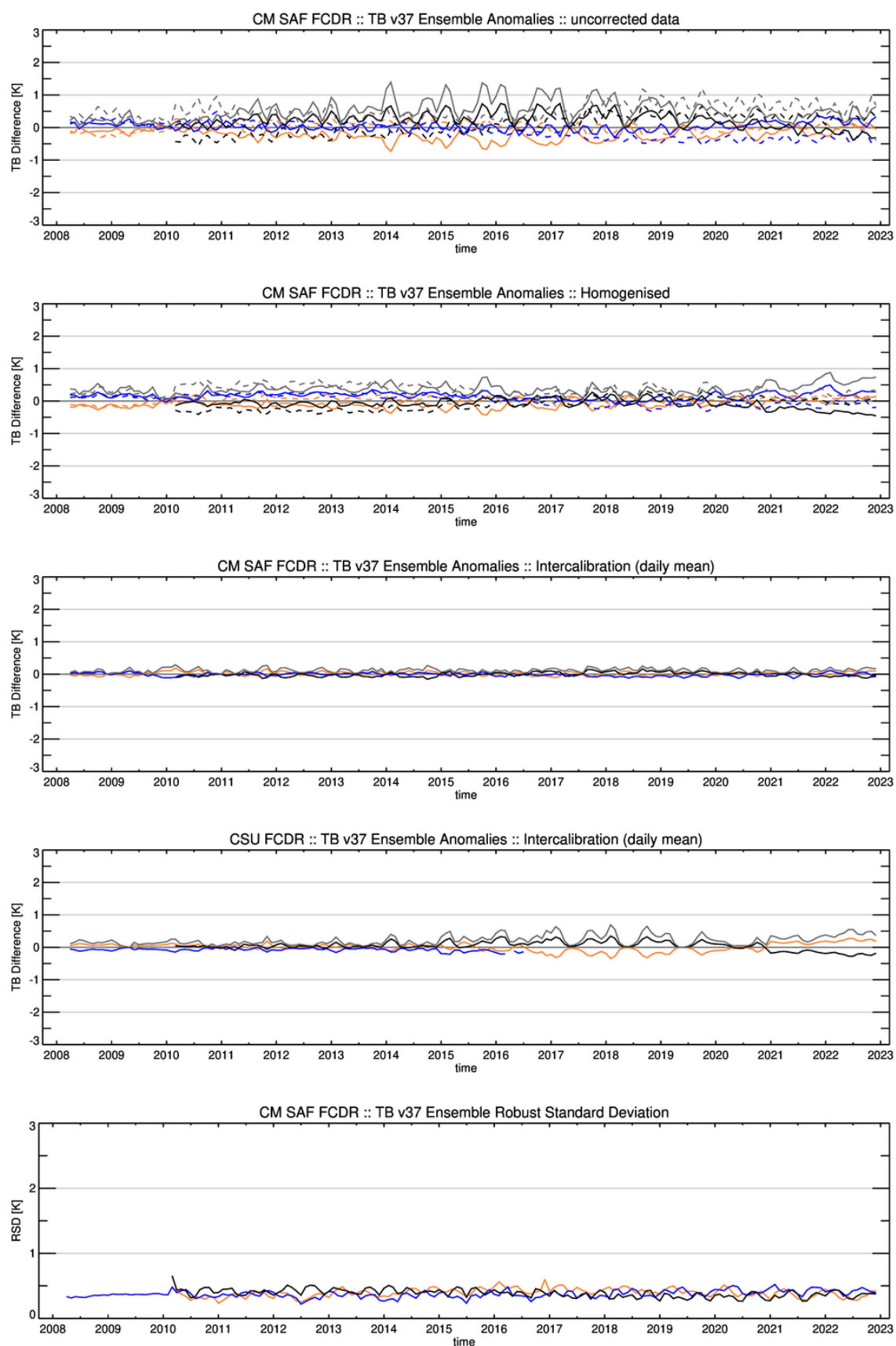


Figure 3-7: Same as Figure 3-4, but for SSM/I & SSMIS channel 37v GHz.


	Validation Report Microwave Imager Radiance FCDR R4.1 SSMIS Brightness Temperatures	Doc. No: SAF/CM/DWD/VAL/FCDR_MWI_CND Issue: 1.0 Date: 2023-08-09
---	--	--

Table 3-9: Statistics of the ensemble anomalies for SSMIS channel 37v GHz. The first block shows the original RDR with EIA normalized, the second block the CM SAF FCDR and the last block the CSU FCDR.

	F16	F17	F18
Bias [K]	-0.03	+0.11	-0.08
RSD [K]	0.40	0.39	0.42
MAD [K]	0.27	0.28	0.29
max absolute inter-sensor Bias [K]	0.14	0.17	0.17
Bias [K]	+0.02	-0.01	0.00
RSD [K]	0.39	0.38	0.39
MAD [K]	0.27	0.26	0.26
max absolute inter-sensor Bias [K]	0.03	0.02	0.03
Trend [K/dec]	+0.02 ($\alpha > 30\%$)	-0.03 ($\alpha > 30\%$)	+0.05 ($\alpha > 30\%$)
Bias [K]	+0.01	-0.08	+0.04
RSD [K]	0.38	0.36	0.41
MAD [K]	0.26	0.25	0.28
max absolute inter-sensor Bias [K]	0.10	0.14	0.14

Table 3-10: Statistics of instrument differences for SSMIS channel 37v GHz. The numbers represent percentiles of absolute differences less than 1K, 2K, and 3K of all individual monthly mean grid boxes between two instruments.

	F16	F17	F18
F16		81.0 96.7 99.3	81.0 96.8 99.4
F17			82.2 97.1 99.5

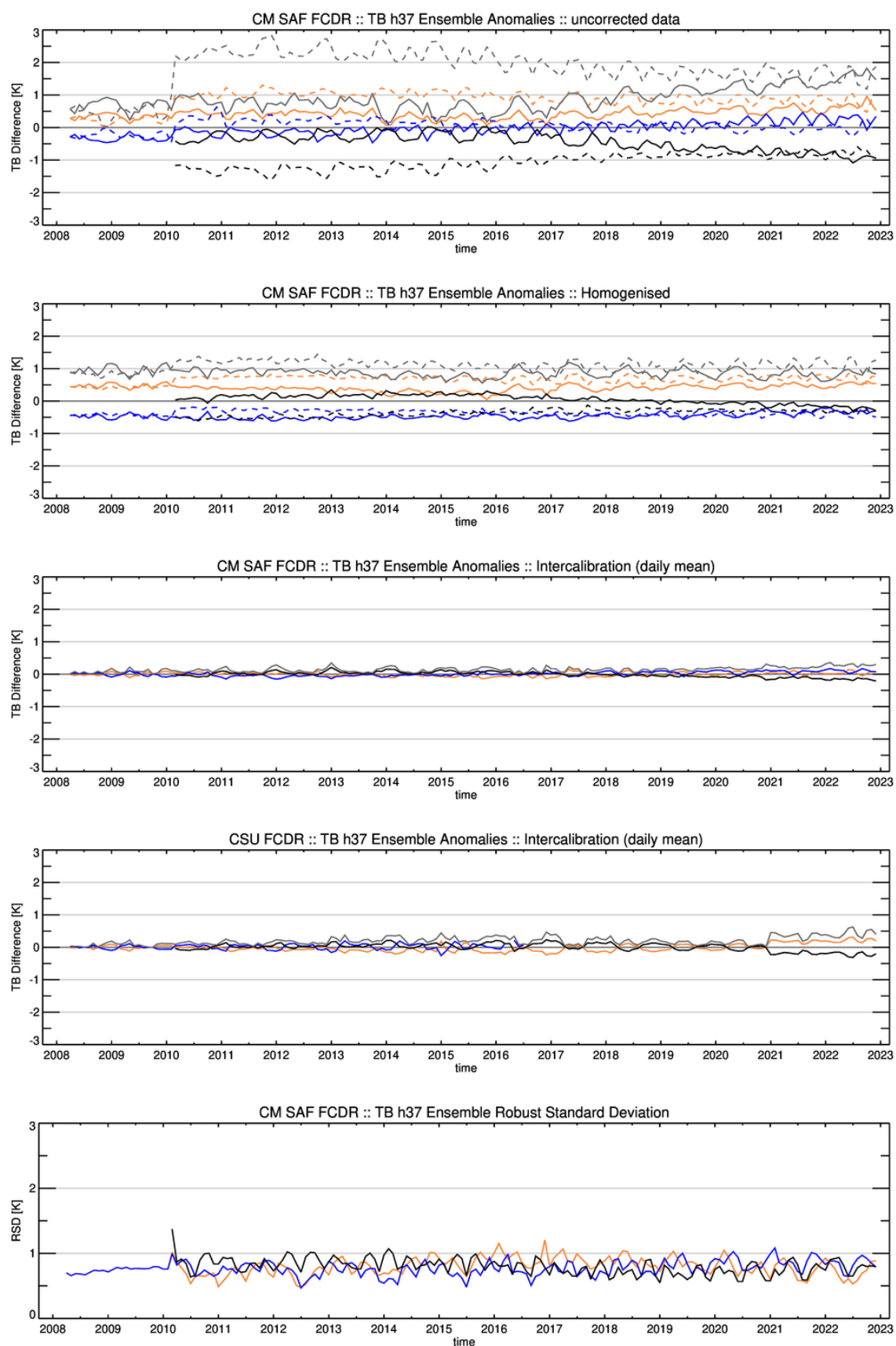


Figure 3-8: Same as Figure 3-4, but for SSM/I & SSMIS channel 37h GHz.

Table 3-11: Statistics of the ensemble anomalies for SSMIS channel 37h GHz. The first block shows the original RDR with EIA normalized, the second block the CM SAF FCDR and the last block the CSU FCDR.

	F16	F17	F18
Bias [K]	+0.54	-0.41	-0.15
RSD [K]	0.80	0.78	0.80
MAD [K]	0.70	0.63	0.55
max absolute inter-sensor Bias [K]	0.94	0.94	0.71
Bias [K]	0.00	+0.01	-0.02
RSD [K]	0.79	0.77	0.80
MAD [K]	0.53	0.52	0.54
max absolute inter-sensor Bias [K]	0.02	0.02	0.02
Trend [K/dec]	0.01 ($\alpha > 30\%$)	+0.12 ($\alpha > 30\%$)	-0.18 ($\alpha > 5\%$)
Bias [K]	0.00	+0.01	-0.01
RSD [K]	0.75	0.80	0.78
MAD [K]	0.50	0.54	0.52
max absolute inter-sensor Bias [K]	0.06	0.06	0.03

Table 3-12: Statistics of instrument differences for SSMIS channel 37h GHz. The numbers represent percentiles of absolute differences less than 1K, 2K, and 3K of all individual monthly mean grid boxes between two instruments.

	F16	F17	F18
F16		53.4 80.4 91.7	52.7 80.2 91.8
F17			54.0 81.4 92.5

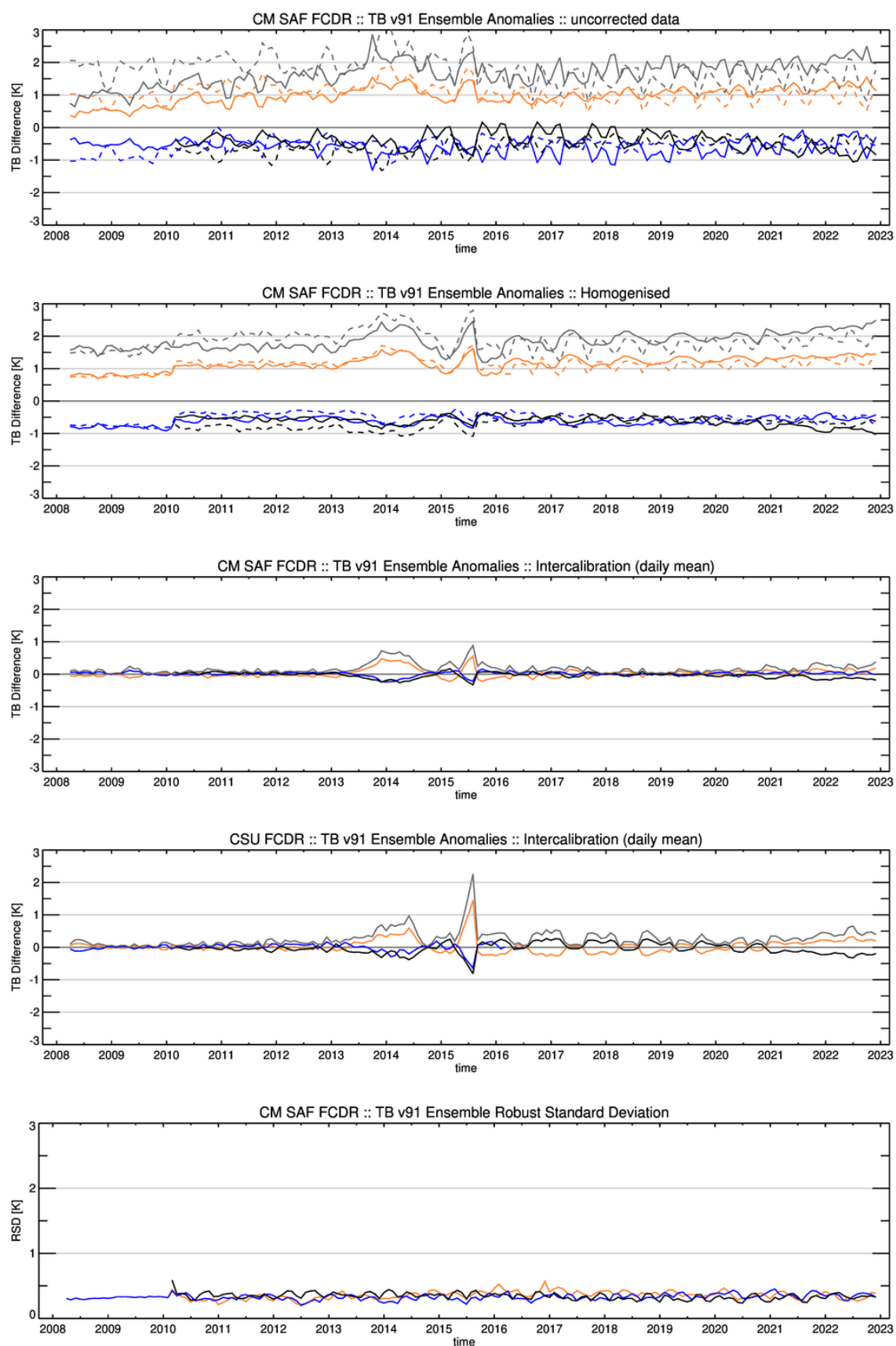


Figure 3-9: Same as Figure 3-4, but for SSMIS channel 91v GHz.

Table 3-13: Statistics of the ensemble anomalies for SSMIS channel 91v GHz. The first block shows the original RDR with EIA normalized, the second block the CM SAF FCDR and the last block the CSU FCDR.

	F16	F17	F18
Bias [K]	+1.14	-0.57	-0.66
RSD [K]	0.43	0.37	0.37
MAD [K]	1.14	0.58	0.67
max absolute inter-sensor Bias [K]	1.86	1.70	1.86
Bias [K]	+0.01	+0.01	-0.03
RSD [K]	0.37	0.34	0.35
MAD [K]	0.25	0.23	0.24
max absolute inter-sensor Bias [K]	0.06	0.04	0.06
Trend [K/dec]	+0.08 ($\alpha > 30\%$)	0.00 ($\alpha > 30\%$)	-0.09 ($\alpha > 30\%$)
Bias [K]	+0.03	0.00	-0.04
RSD [K]	0.37	0.36	0.39
MAD [K]	0.25	0.24	0.26
max absolute inter-sensor Bias [K]	0.07	0.08	0.08

Table 3-14: Statistics of instrument differences for SSMIS channel 91v GHz. The numbers represent percentiles of absolute differences less than 1K, 2K, and 3K of all individual monthly mean grid boxes between two instruments.

	F16	F17	F18
F16		84.7 98.2 99.7	84.2 98.3 99.8
F17			87.5 98.7 99.8

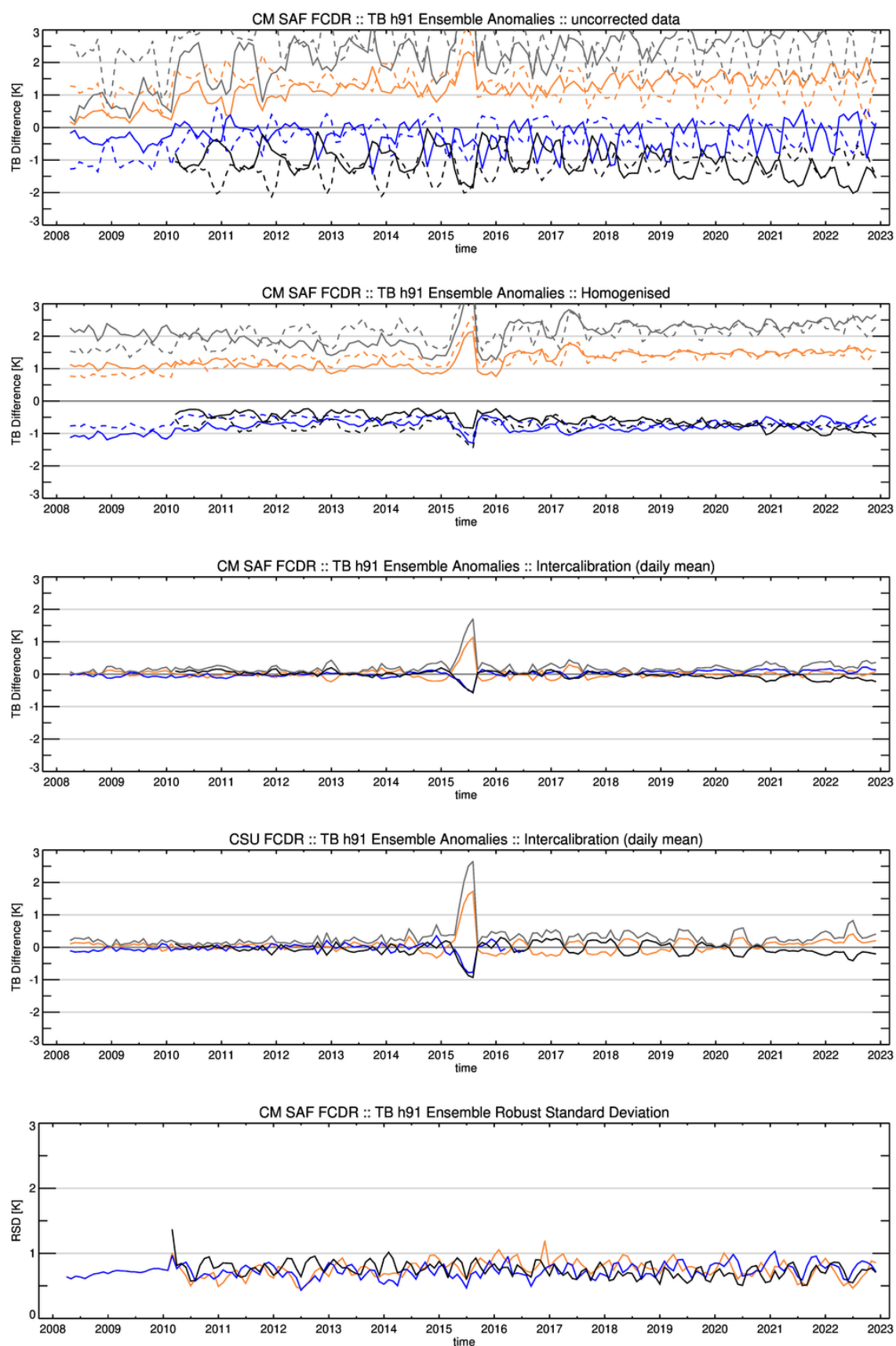


Figure 3-10: Same as Figure 3-4, but for SSMIS channel 91h GHz.

Table 3-15: Statistics of the ensemble anomalies for SSMIS channel 91h GHz. The first block shows the original RDR with EIA normalized, the second block the CM SAF FCDR and the last block the CSU FCDR.

	F16	F17	F18
Bias [K]	+1.26	-0.73	-0.65
RSD [K]	0.85	0.76	0.77
MAD [K]	1.29	0.81	0.76
max absolute inter-sensor Bias [K]	1.99	1.99	1.99
Bias [K]	+0.01	+0.01	-0.03
RSD [K]	0.76	0.73	0.74
MAD [K]	0.52	0.50	0.50
max absolute inter-sensor Bias [K]	0.03	0.04	0.04
Trend [K/dec]	-0.01 ($\alpha > 30\%$)	0.14 ($\alpha > 5\%$)	-0.16 ($\alpha > 5\%$)
Bias [K]	+0.06	-0.03	-0.05
RSD [K]	0.72	0.74	0.75
MAD [K]	0.49	0.50	0.51
max absolute inter-sensor Bias [K]	0.10	0.08	0.10

Table 3-16: Statistics of instrument differences for SSMIS channel 91h GHz. The numbers represent percentiles of absolute differences less than 1K, 2K, and 3K of all individual monthly mean grid boxes between two instruments.

	F16	F17	F18
F16		54.8 82.6 93.6	54.9 82.8 93.8
F17			56.9 84.4 94.7

3.3 Comparison against GMI

Another type of evaluation of the SSMIS FCDR is to analyse the brightness temperatures relative to another independent, stable observation. This option became possible with the availability of data from the GPM Microwave Imager (GMI). The Global Precipitation Measurement (GPM) platform was launched end of February 2014. The platform is in a non-synchronous orbit, with an inclination of 65 degrees. This type of orbit allows a sampling of all local Earth times in about two weeks, covering the Earth within about ± 70 degree latitude.

The GMI is a dual-polarization, conical-scanning, passive microwave radiometer. The principle design of the instrument and the strict calibration accuracy enables it to serve as a high-quality in-orbit reference instrument. More information about the GMI instrument is given by Draper et al. (2015).

The GMI centre frequencies are shifted relative to the SSMIS frequencies. The SSMIS-like channels are centred at 18.7, 23.8, 36.5 and 89.0 GHz and are sampled at horizontal and vertical polarization, except the 23.8 GHz channel. GMI level-1 data records are available at the NASA PPS data server (<https://arthurhou.pps.eosdis.nasa.gov/>). Due to the shift in the channel frequencies, an absolute difference between the observations from GMI and SSMIS is expected. However, all SSMIS instruments should depict the same difference after all calibration offsets are applied.

The comparison against GMI is done, similar to the inter-sensor evaluation, for monthly mean values. The instantaneous observations from all instruments are gridded into daily global 1° equal angle grids. As the GMI is in a non-synchronous orbit, ascending and descending orbits are directly compiled into daily mean gridded fields for each channel. The monthly mean anomalies between the SSMIS T_B and the GMI $T_{B,GMI}$ are then calculated for each grid cell. Following the notation established in section 3.2.2, the brightness temperature anomalies at each grid point g , time step t and instruments s are then defined as:

$$\Delta T_B(s, t, g) = T_B(s, t, g) - T_{B,GMI}(t, g). \quad \text{Equation 6}$$

In order to compare the characteristics of the time series for both instruments, the global median $\overline{\Delta T_{B,s}}(t)$ is derived for each month. The time series of these anomalies are presented in Figure 3-11 to Figure 3-14. All figure panels contain two images for each frequency and polarisation with the global monthly mean values of:

1. T_B anomalies with intrusion correction, reflector emissivity correction and EIA normalization applied,
2. T_B anomalies of the final CM SAF FCDR, (inter-sensor calibration offsets and solar calibration correction offsets are applied).

As expected, the final differences can be quite large due to the differences in the centre frequency of the compared channels, which is not adjusted. The largest differences are found for the 19.35 GHz (18.7 GHz) channels with about 6 K and 9 K.

However, after the application of the inter-sensor correction offsets to the SSMIS brightness temperatures, the observed differences between the three sensors are removed.

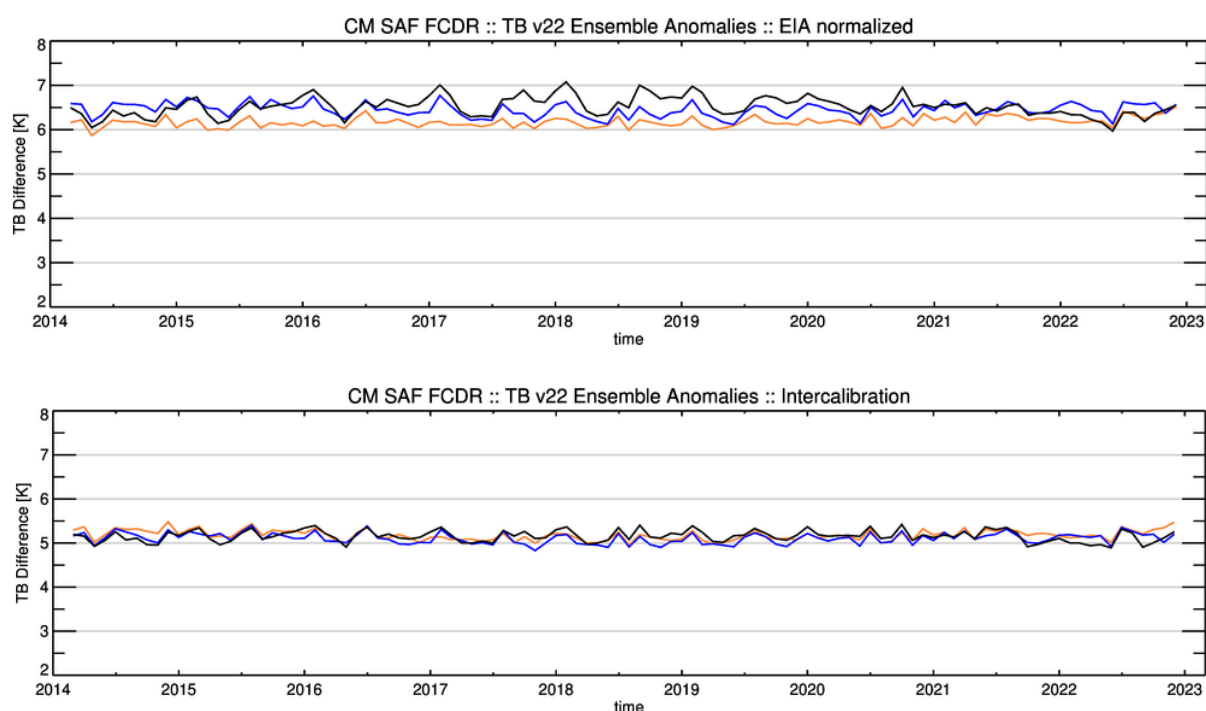


Figure 3-11: Time series of global monthly mean anomalies of SSMIS minus GMI brightness temperatures at 22 GHz. The upper panel shows the homogenised data records and the lower panel depicts the inter-sensor calibrated SSMIS data record. Colours are as in Figure 3-1.

A regular seasonal signal is visible for the uncorrected the SSMIS_{F18} data, most pronounced in the 22v and the 37v channels. This feature also corresponds to a seasonal variation found in the inter-sensor validation (see section 3.2.3). However, by comparing to an independent data record, it becomes clear that this variation is mainly caused by the SSMIS_{F18}. The newly developed solar calibration correction (see ATBD [RD 1]) removes this issue. Also, the previously identified anomalies in the 91 GHz (see section 3.2.3) are clearly visible in 2014 and 2015.

A thorough trend analysis is hampered by the short time period. However, consistent with the results from the inter-sensor evaluation in section 3.2, some of the SSMIS_{F18} channels depict a small negative trend at the end of the covered time period. This is most pronounced in the 37h and 91h channels. Contrary to this, the SSMIS_{F16} and SSMIS_{F17} channels 19h, 37h and 91h show a small positive trend over time. This could be caused by the different orbits of the SSMIS (sun-synchronous) and the GMI (non-sun-synchronous) platforms.

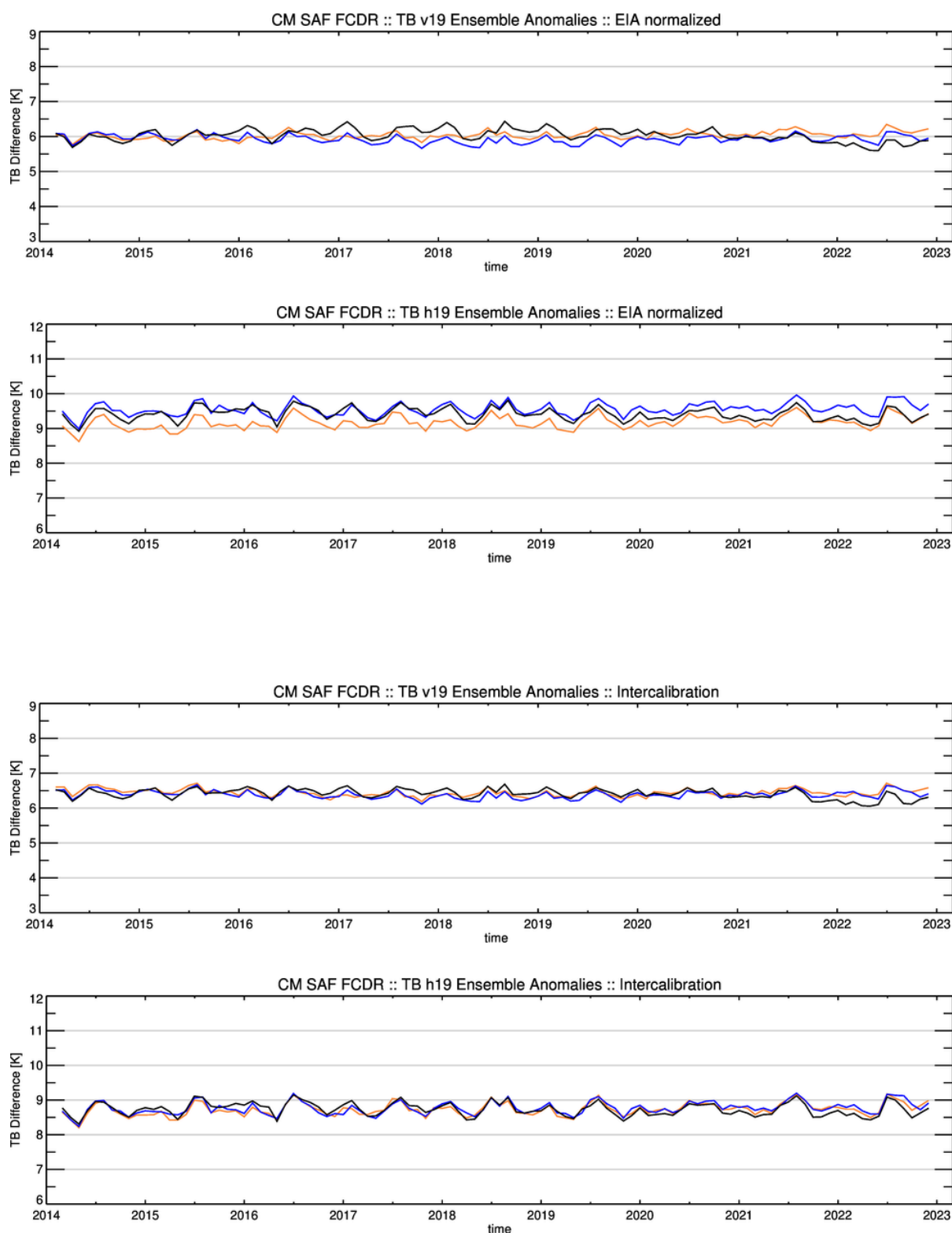


Figure 3-12: Time series of global monthly mean anomalies of SSMIS minus GMI brightness temperatures at 19 GHz. The upper two panels show the homogenised data records and the two lower panels depict the inter-sensor calibrated SSMIS data record. Colours are as in Figure 3-1.

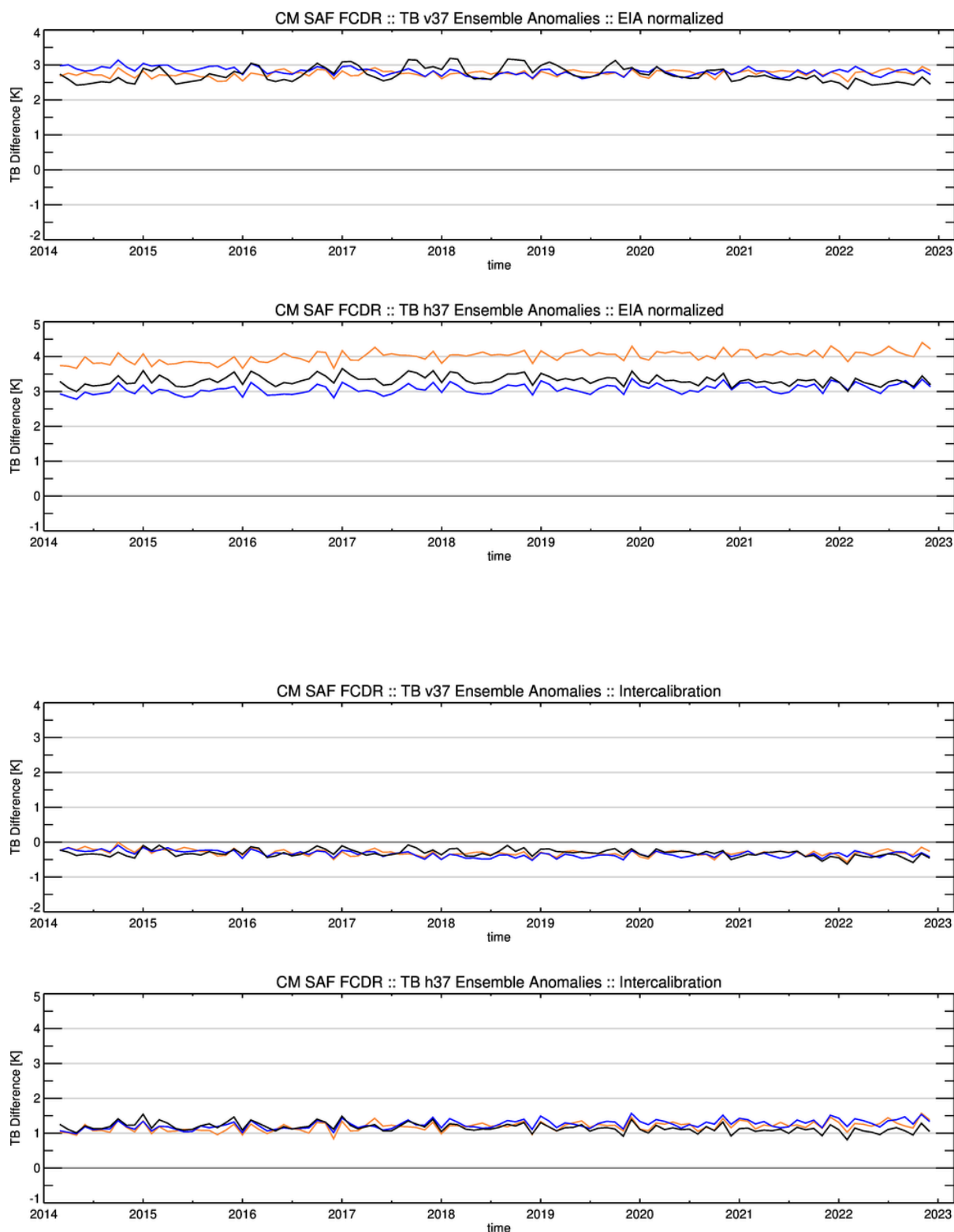


Figure 3-13: Time series of global monthly mean anomalies and SSMIS minus GMI channels at 37 GHz. The upper two panels show the homogenised data records and the two lower panels depict the inter-sensor calibrated SSMIS data record. Colours are as in Figure 3-1.

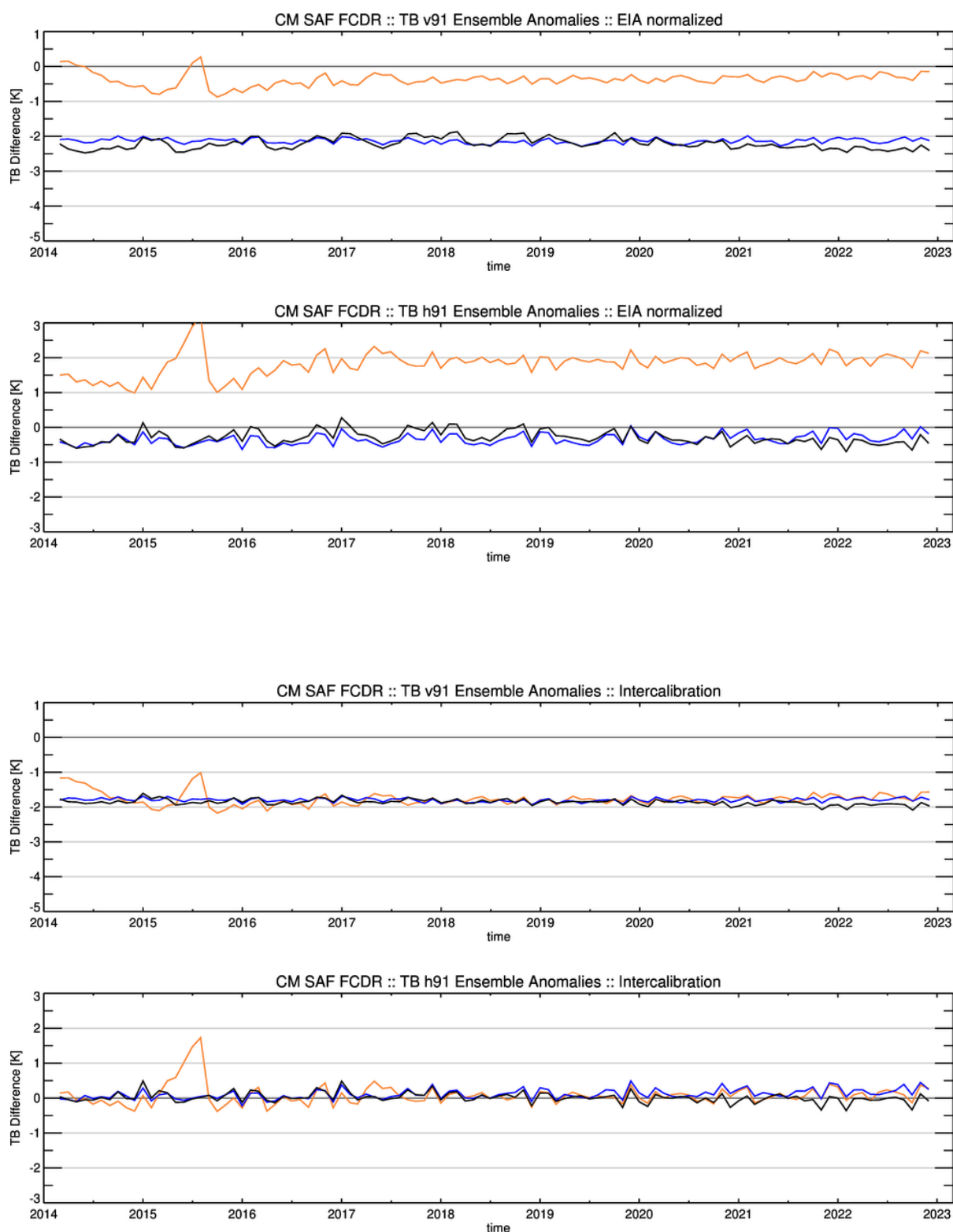


Figure 3-14: Time series of global monthly mean anomalies and SSMIS minus GMI channels at 91 GHz. The upper two panels show the homogenised data records and the two lower panels depict the inter-sensor calibrated SSMIS data record. Colours are as in Figure 3-1.

3.4 Evaluation of brightness temperature differences against reanalysis

Additionally, to the inter-sensor comparison in section 3.2, a more complete analysis of each individual channel across the sensors for the complete time period was conducted. The idea is to derive an improved characterisation of the long-term FCDR stability, using independent reanalysis data records. However, this approach is hampered due to several constraints. The basic assumptions are that the reanalysis is independent of the observations, stable in time and does cover the complete time period of the FCDR. Moreover, the uncertainties in the applied radiative transfer model and the surface emissivity model should be well behaved and characterised. However, there is actually no reanalyses available fulfilling all the constraints.

The first choice to evaluate the FCDR is to use the ERA-20C reanalysis similar to the SMMR inter-calibration and evaluation, as it does not assimilate any satellite observations, being independent from the FCDR. However, the covered time period ends already in 2010. This does not allow a complete analysis of the transition from SSM/I to SSMIS with SSMIS_{F18} data becoming available in 2010. Therefore, also the ERA5 reanalysis (Hersbach et al., 2020) was used in the evaluation process, although it does not fulfil our requirements. Firstly, it is not independent as it assimilates SSM/I and SSMIS data records. Moreover, the SSM/I part of this CM SAF FCDR is assimilated. Secondly, it is also not stable in time, as the composition of the assimilated observation systems is changing over time.

A serious limitation in the comparison is the large uncertainty of surface emissivity models over land, sea-ice and snow covered surfaces due to unknown surface emissivities. Also, the strong diurnal cycle over land is likely not fully resolved by the reanalysis. Additionally, rainy and cloudy scenes increase the uncertainty of the radiative transfer model due to scattering effects of the water droplets. In order to minimize these influences, only cloud-free and lightly cloudy scenes over water surfaces are selected for the match-up data sets. However, this practically limits this comparison to the cold end of the natural spectrum and no conclusion can be drawn for the scene dependence or the warm end of the spectrum.

Brightness temperatures at the top of the atmosphere are calculated for the filtered data record with RTTOV 11.2 (Saunders et al. 2013) and the surface emissivity with FASTEM 6 (Meunier et al. 2014). Profiles from ERA5 are available every hour. However, in order to limit the overall data volume, the same temporal sampling of 3 hours is selected. The simulations are done for the entire time period covered by the FCDR. As this study focuses on the FCDR extension, only the SSMIS part is analysed and discussed here. In order to reduce the uncertainty in the observed differences, the match-up data is then gridded into daily global 1° equal angle grids, separately for ascending and descending orbits.

The monthly mean anomalies between the observation T_B and the model T_{BM} are calculated for each grid cell. Following the notation established in section 3.2.2, the anomalies at each grid point are then defined as:

$$\Delta T_B(s, t, g) = T_B(s, t, g) - T_{BM}(s, t, g). \quad \text{Equation 7}$$

In order to compare the characteristics of the time series for all instruments and both reanalysis, global median ($\overline{\Delta T_{B,s}}(t)$) and robust standard deviation ($RSD_s(t)$) are derived for each month.

3.5 Evaluation results

The time series for AM/PM global monthly mean anomalies are shown for all FCDR channels in Figure 3-16 to Figure 3-23 and the robust standard deviations (RSD) for the vertically polarised channels in in Figure 3-24. The RSD time series for the horizontally polarized channels are not shown here, as the trends are very similar to the vertically polarised channels. All mean figure panels contain two images with global monthly mean time series of:

1. anomalies between raw data records (with reflector emissivity correction, intrusion correction applied, and EIA normalisation applied) and ERA5,
2. anomalies between inter-calibrated data records (all corrections applied) and ERA5.

In order to perform a linear trend analysis for the complete SSMIS period, all individual instrument anomalies are averaged to provide a single data record for a specific frequency. The long-term trend is then estimated using Equation 5 with these mean anomalies and summarized in Table 3-17.

The general conclusions from these comparisons are very similar to the results from the inter-sensor comparisons. Also, the channels 37h and 91h of the SSMIS_{F18} depict the same trend at the end of the covered time period, consistent with the findings in section 3.2 and 3.3.

The applied inter-calibration effectively removes the observed differences between the instruments. The residual TB inter-satellite difference is in the order of 0.1 to 0.2 K after applying the inter-sensor calibration for most of the channels and instrument combinations. The final inter-sensor differences stay well within 1 K optimum bias criteria over the whole time-period.

The results of this linear trend analysis must be carefully interpreted because the reanalysis is not a stable reference. Observed trends can be caused by the reanalysis or the FCDR data records. Overall, most channels depict a positive decadal trend within the SSMIS era

Table 3-17: Estimated trends for global monthly mean differences between the simulated brightness temperatures from ERA5 and the combined inter-calibrated FCDR.

Channel	Trend ERA5 [K/dec]	
v19	0.07	$\alpha > 30\%$
h19	0.11	$\alpha > 30\%$
v22	-0.06	$\alpha > 30\%$
v37	0.00	$\alpha > 30\%$
h37	0.13	$\alpha > 30\%$
v85	0.16	$\alpha > 30\%$
h85	0.23	$\alpha > 30\%$
v91	0.16	$\alpha > 5\%$
h91	0.22	$\alpha > 30\%$

(see Table 3-17) This trend is stronger for the horizontally polarized channels (~ 0.2 K/decade) and smaller for the vertically polarized channels 0.1 K/decade). This trend, consistent across all SSMIS instruments, starts in 2020 and is accompanied by a decrease in the RSD (see Figure 3-24). As this behaviour is very consistent for all channels, follow each other very close, and the RSD is dropping, it is more likely that the ERA5 data is changing over time. This would then result in an improving overall agreement between ERA5 and the SSMIS FCDR TBs but at a different level of the global mean bias value.

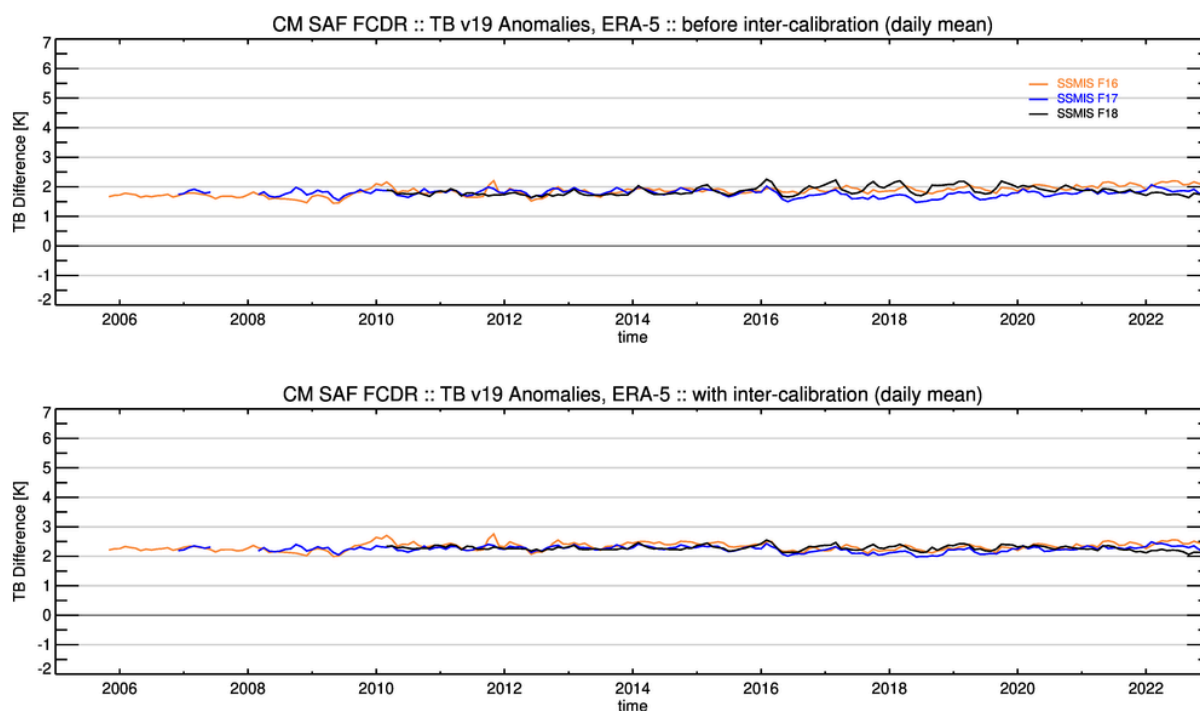


Figure 3-15: Time series of global monthly mean TB differences for the 19v GHz channel between the FCDR SSMIS instruments and ERA5. Colours for the instrument are F16 (orange), F17 (blue), F18 (black).

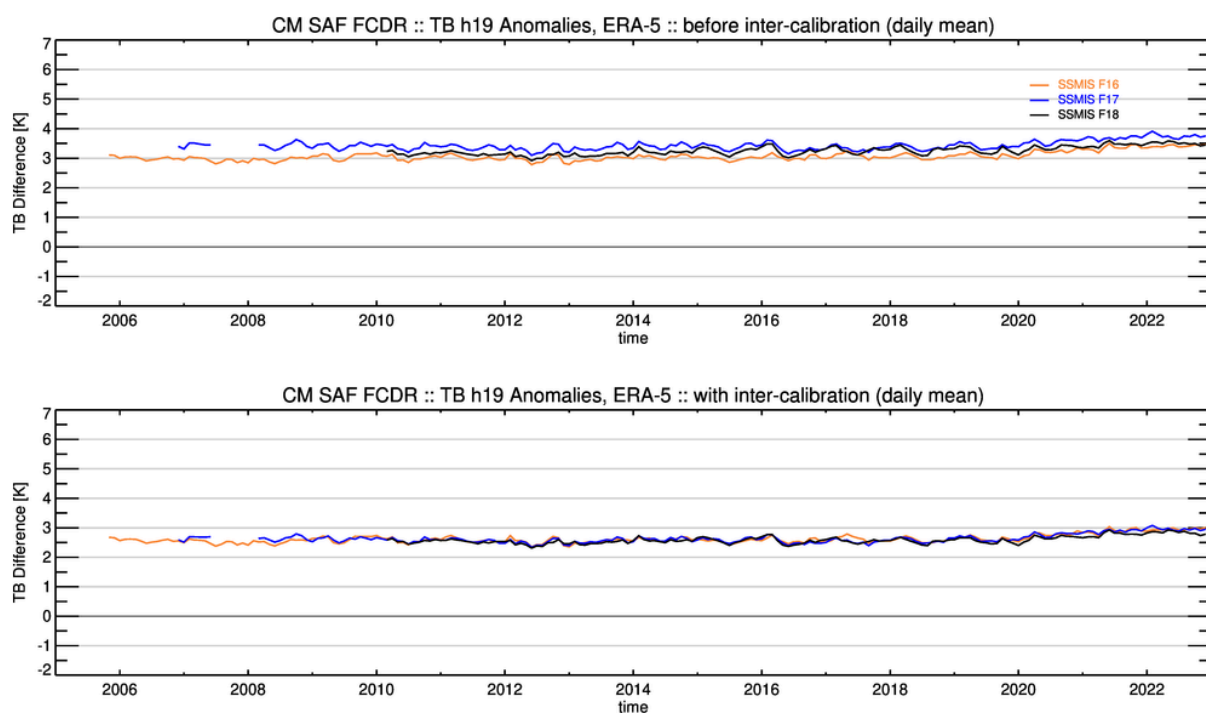


Figure 3-16: Same as Figure 3-15 but for 19h GHz.

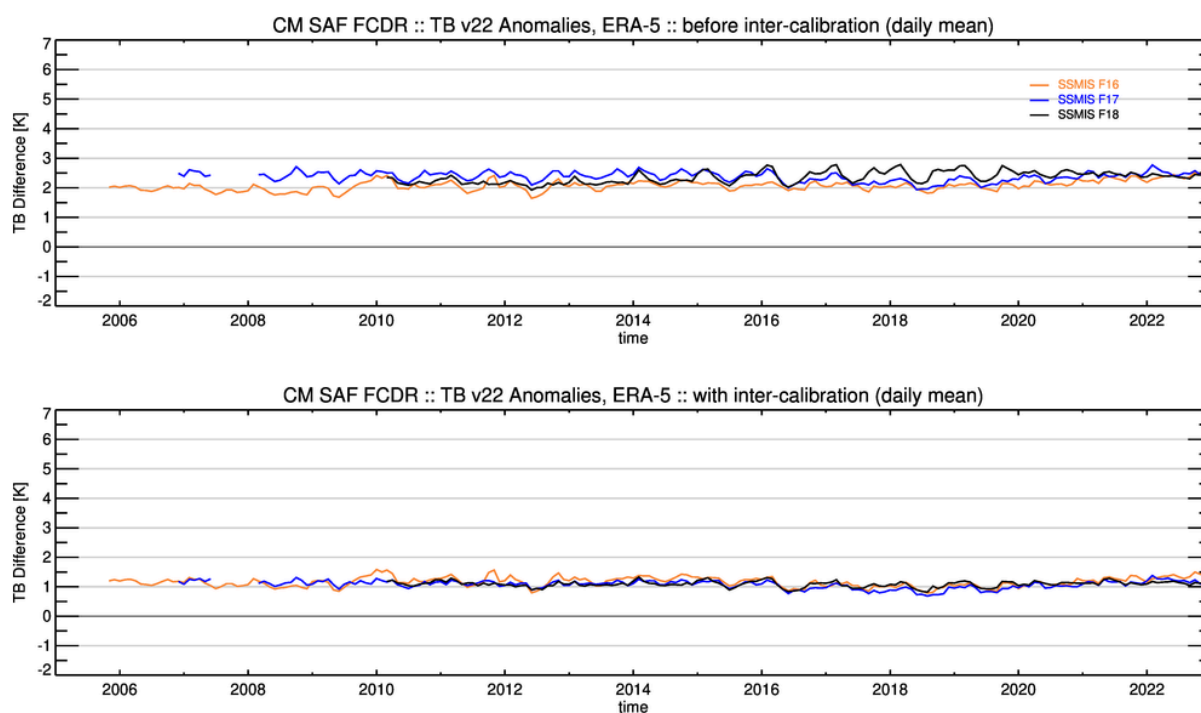


Figure 3-17: Same as Figure 3-15 but for 22v GHz.

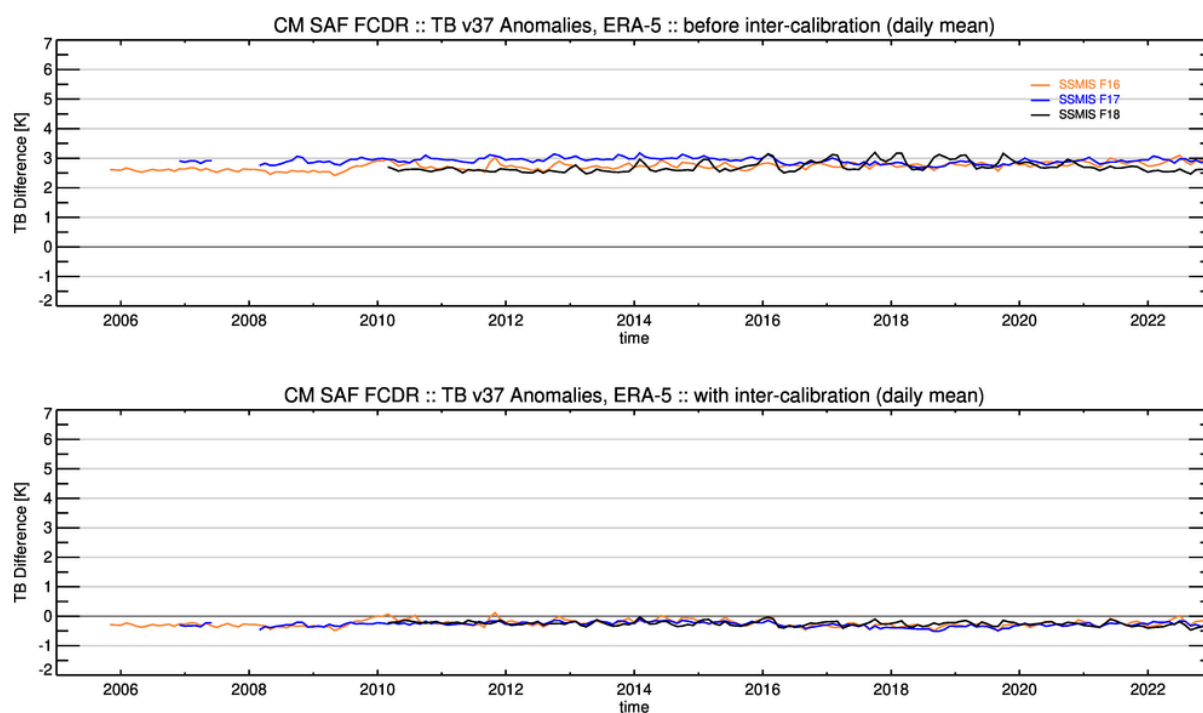


Figure 3-18: Same as Figure 3-15 but for 37v GHz.

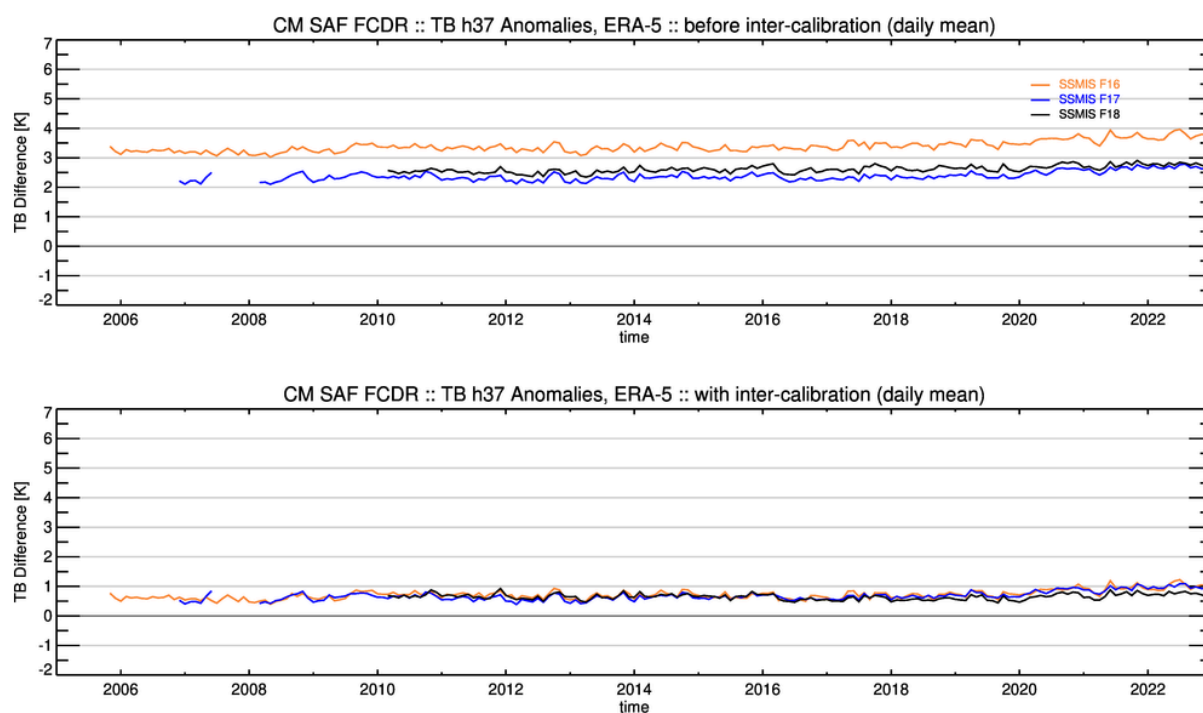


Figure 3-19: Same as Figure 3-15 but for 37h GHz.

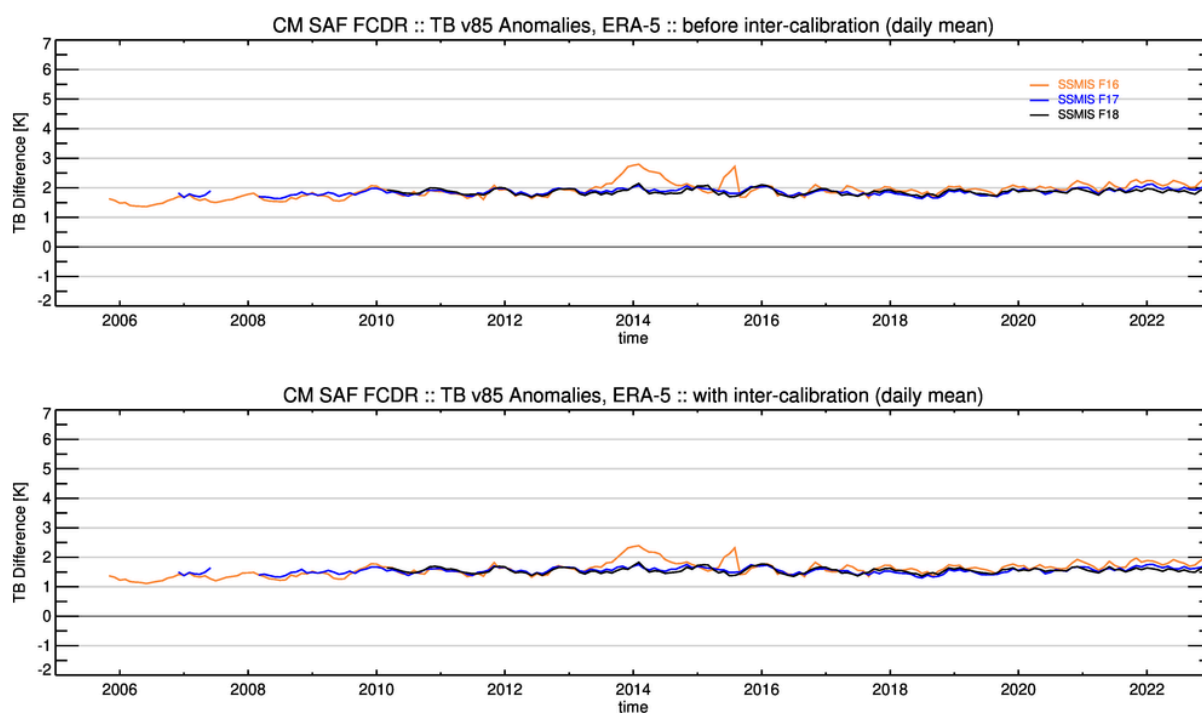


Figure 3-20: Same as Figure 3-15 but for 85v GHz.

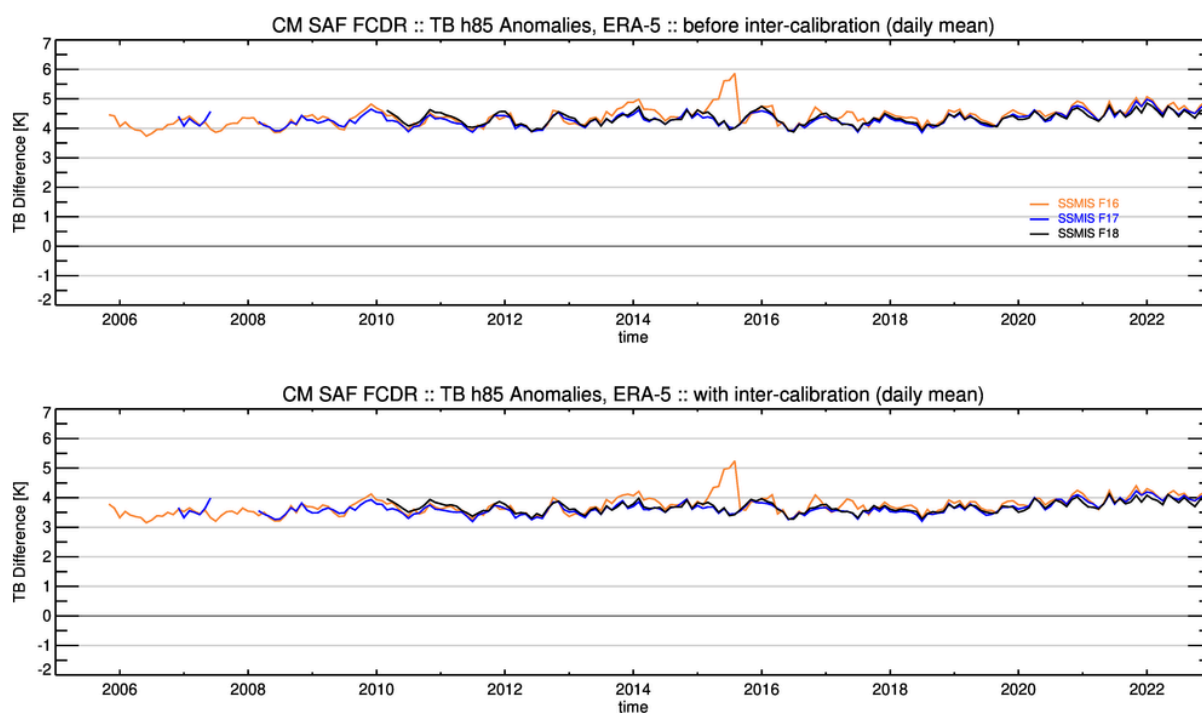


Figure 3-21: Same as Figure 3-15 but for 85h GHz.

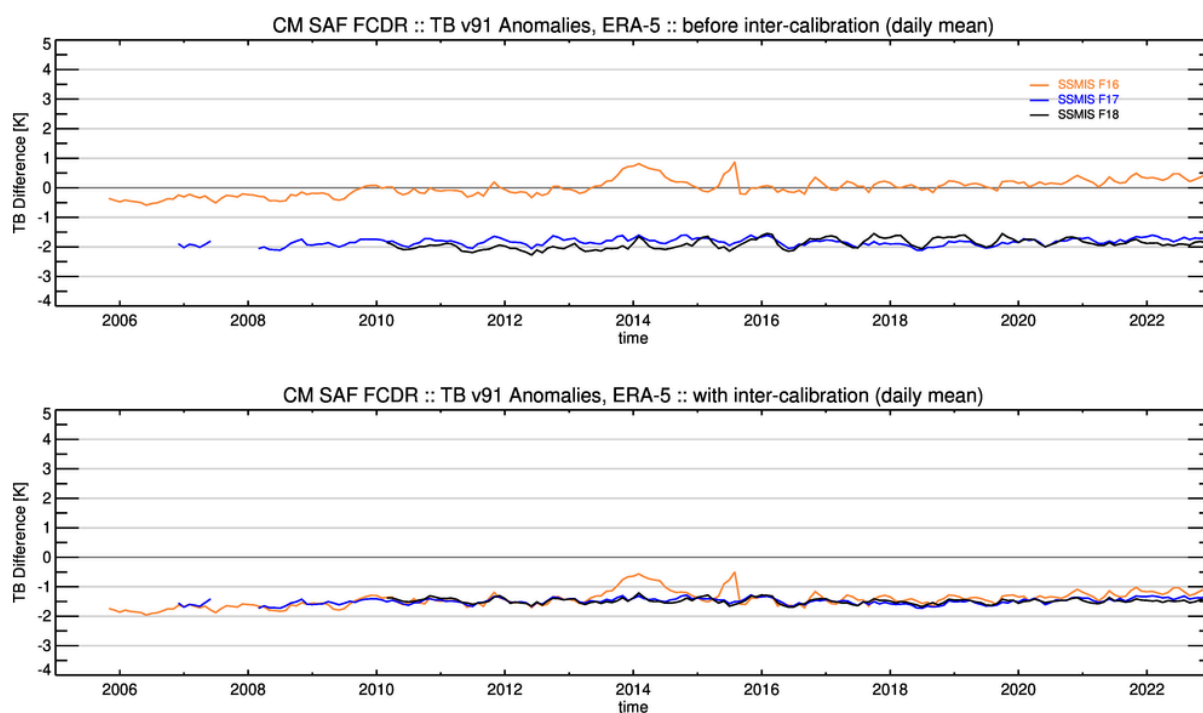


Figure 3-22: Same as Figure 3-15 but for 91v GHz.

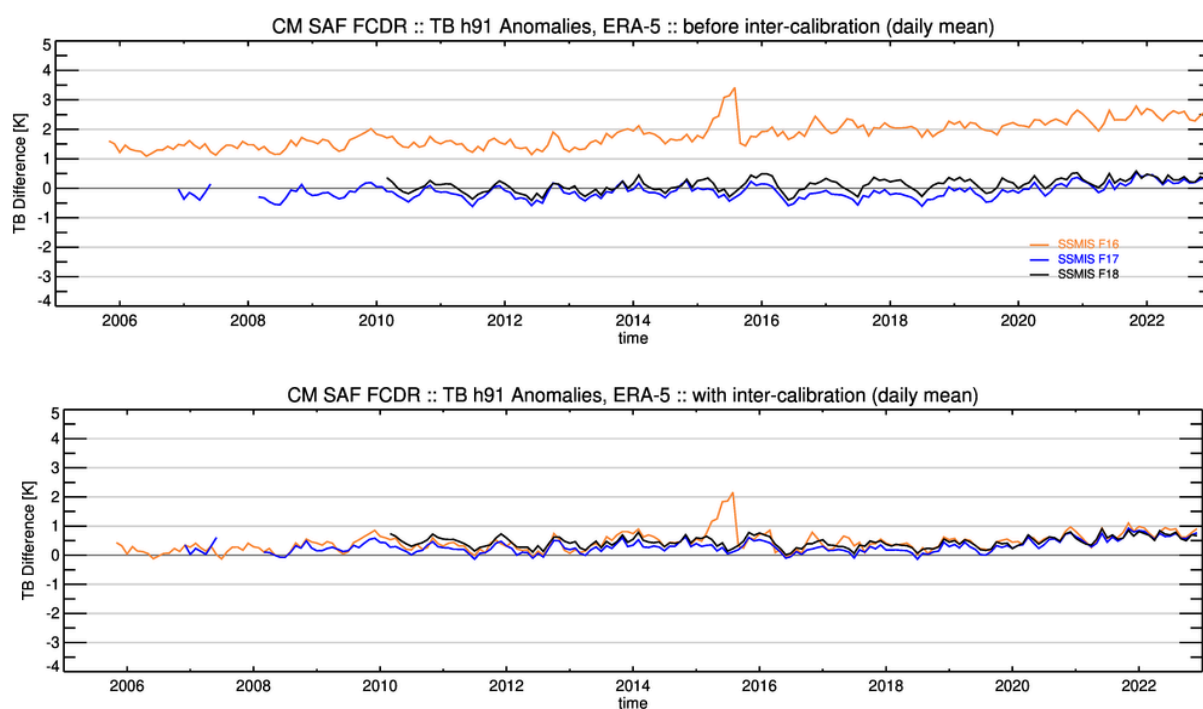


Figure 3-23: Same as Figure 3-15 but for 91h GHz.

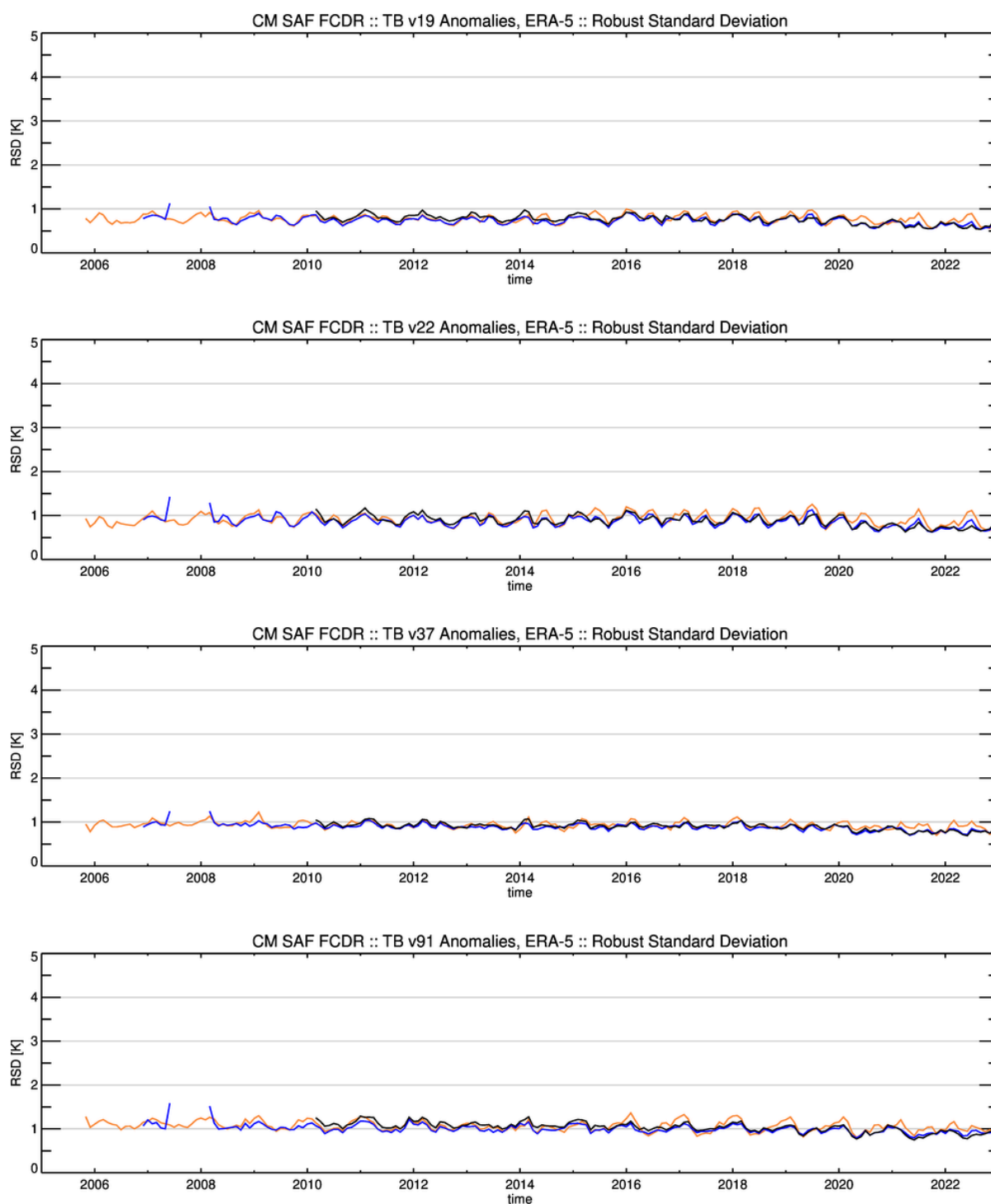


Figure 3-24: Time series of robust standard deviation of global monthly mean TB differences for the channels 19v, 22v, 37v, and 85v GHz between the CM SAF FCDR and ERA5.

4 Conclusions

The CM SAF FCDR extension (release 4.1) of SSMIS brightness temperatures has been evaluated to analyse the homogeneity, consistency and the stability of the developed inter-calibration model. The CM SAF FCDR has been compared to the original RDR and another available FCDR from CSU. The main distinction between both FCDRs is found in the applied inter-calibration method. The inter-calibration method developed for the CM SAF FCDR explicitly includes all possible surface types to account for the entire natural distribution of brightness temperatures from radiometric cold scenes (rain-free ocean) to radiometric warm scenes (vegetated land surfaces). In contrast to this, the inter-calibration method developed at CSU uses only rain-free brightness temperatures range observed by the TMI instrument because this is used as transfer standard. This limits the CSU inter-calibration to the radiometric cold end of the natural spectrum and hampers a consideration of the full range of possible scene dependencies.

The consistency and homogeneity of FCDR and the uncorrected RDR were statistically analysed to demonstrate the improvement of the re-processed data records and compliance with the user requirements. Those requirements are defined in terms of mean absolute systematic inter-satellite deviations and decadal stability. The stability and homogeneity have also been tested by comparing the observed brightness temperatures against GMI observations and against modelled brightness temperatures using the ERA5 reanalysis.

The observed differences in the RDR range between 0.5 K to 2.5 K, depending on channel and instrument, but generally the differences are smaller within the SSMIS series as compared to the inter-sensor difference to the SSM/I family. The overall mean differences in the CM SAF FCDR between the different sensors have been reduced to below 0.1 K, which is a significant improvement over the RDR. The mean RSD for all channels and instruments has been significantly reduced. The observed remaining variability in the inter-calibrated TBs is mainly caused by the natural variability due to overpass time differences and sampling differences. No trends above the target criterium can be observed in the inter-sensor differences.

Comparing the FCDR against modelled brightness temperatures confirmed the results from the inter-sensor differences. However, it is still difficult to interpret the results in terms of temporal stability, as also the reanalysis is not a stable reference.

The observed trends in the last years of the covered time period for some of the SSMIS_{F18} channels are most likely related to limitations of the applied solar correction. The parameters of this correction have been fitted for the time period until 2020. Applying this correction for a time period with solar angles beyond the fitted range can result in an underestimation of the solar effects in the TBs. The solar correction is performing better for the other channels of the SSMIS_{F18}, where the trend, which is visible in the uncorrected data, is effectively removed. These trends, where they persist, must be monitored and the solar correction should be updated for the next release.

Finally, it can be concluded that this FCDR is providing a greatly improved quality of the and SSMIS brightness temperatures as compared to original raw data records and fulfils the aimed requirements. It extends the current FCDR until end of 2022. The final combined FCDR provides inter-calibrated brightness temperatures for the time period from 1978 to 2022.

5 References

Andersson, A., Fennig, K., Klepp, C., Bakan, S., Graßl, H., and Schulz, J.: The Hamburg Ocean Atmosphere Parameters and Fluxes from Satellite Data – HOAPS-3, *Earth Syst. Sci. Data*, 2, 215-234, doi:10.5194/essd-2-215-2010, 2010.

Andersson, A., C. Klepp, K. Fennig, S. Bakan, H. Graßl, and J. Schulz: Evaluation of HOAPS-3 ocean surface freshwater flux components, *Journal of Applied Meteorology and Climatology*, 50, 379-398, doi:10.1175/2010JAMC2341.1, 2011.

Berg, W., Sapiano, M. R. P. ; Horsman, J. ; Kummerow, C., 2012: Improved Geolocation and Earth Incidence Angle Information for a Fundamental Climate Data Record of the SSM/I Sensors, *IEEE Transactions on Geoscience and Remote Sensing*, Early online release, doi: 10.1109/TGRS.2012.2199761.

Berg, W., 2013: Fundamental Climate Data Record (FCDR) for the Special Sensor Microwave Imager/Sounder (SSMIS), Climate Algorithm Theoretical Basis Document (C-ATBD), CDR Program Document Number: CDRP-ATBD-0338

Draper, D. W., D. Newell, F. J. Wentz, S. Krimchansky, and G. M. Skofronick-Jackson, 2015: The Global Precipitation Measurement (GPM) Microwave Imager (GMI): Instrument overview and early on-orbit performance. *IEEE Journal of Selected Topics in Applied Earth Observations and Remote Sensing*. doi:10.1109/JSTARS.2015.2403303.

Fennig, K.; Andersson, A.; Schröder, M. (2013): Fundamental Climate Data Record of SSM/I Brightness Temperatures. Satellite Application Facility on Climate Monitoring. DOI:10.5676/EUM_SAF_CM/FCDR_SSMI/V001.

Fennig, K.; Andersson, A.; Schröder, M. (2015): Fundamental Climate Data Record of SSM/I / SSMIS Brightness Temperatures. Satellite Application Facility on Climate Monitoring. DOI:10.5676/EUM_SAF_CM/FCDR_MWI/V002.


Francis, E. A. (1987): Calibration of the Nimbus-7 Scanning Multichannel Microwave Radiometer (SMMR) 1979-1984. Master's Thesis, College of Oceanography, Oregon State University, Corvallis Oregon.

Furhop, R. and Simmer, C.: SSM/I Brightness Temperature Corrections for Incidence Angle Variations, *J. Atmos. Oceanic Technol.*, 13, 246–254, 1996.

Hersbach, H, Bell, B, Berrisford, P, et al. The ERA5 global reanalysis. *Q J R Meteorol Soc.* 2020; 146: 1999– 2049. <https://doi.org/10.1002/qj.3803>

Hollinger, J., Poe, G..A.: Special Sensor Microwave/Imager User's Guide, Naval Research Laboratory Report, Washington DC, 1987.

Kummerow, Christian D., Wesley K. Berg, Chia-Pang Kuo, and NOAA CDR Program, 2022: NOAA Climate Data Record (CDR) of SSMI(S) and AMSR2 Microwave Brightness Temperatures, CSU Version 2. NOAA National Centers for Environmental Information. <https://doi.org/10.25921/E3K5-BW77>. 2023-08-08.

	Validation Report Microwave Imager Radiance FCDR R4.1 SSMIS Brightness Temperatures	Doc. No: SAF/CM/DWD/VAL/FCDR_MWI_CND Issue: 1.0 Date: 2023-08-09
---	--	--

Njoku, E. G. (2003): Nimbus-7 SMMR Pathfinder Brightness Temperatures, Version 1., Boulder, Colorado USA. NASA National Snow and Ice Data Center Distributed Active Archive Center. DOI:10.5067/7Y1XWXT07HH8.

Poli P, and Co-authors (2013): The data assimilation system and initial performance evaluation of the ECMWF pilot reanalysis of the 20th-century assimilating surface observations only (ERA-20C). ERA Report Series 14, September 2013, 59 pp., available from ECMWF, Shinfield Park, Reading. <http://old.ecmwf.int/publications/library/do/references/list/782009>

Schröder, M., M. Lockhoff, J. Forsythe, H. Cronk, T. H. Vonder Haar, R. Bennartz, 2016: The GEWEX water vapor assessment (G-VAP) – results from the trend and homogeneity analysis. J. Applied Meteor. Clim., 1633-1649, 55 (7), doi: /10.1175/JAMC-D-15-0304.1.

Semunegus, H: Remote Sensing Systems Version-6 Special Sensor Microwave/Imager Fundamental Climate Data Record, Climate Algorithm Theoretical Basis Document, Climate Data Record (CDR) Program, CDRP-ATBD-0100, 2011.

6 Glossary

APC	Antenna Pattern Correction
ATBD	Algorithm Theoretical Baseline Document
CM SAF	Satellite Application Facility on Climate Monitoring
CDOP	Continuous Development and Operations Phase
CSU	Colorado State University
DMSP	Defense Meteorological Satellite Program
DWD	Deutscher Wetterdienst (German MetService)
ECI	Earth-centred inertial
ECMWF	European Centre for Medium Range Forecast
ECV	Essential Climate Variable
EIA	Earth Incidence Angle
EPS	European Polar System
ERA-20C	ECMWF Reanalysis of the 20th century
ERA5	ECMWF Reanalysis
EUMETSAT	European Organisation for the Exploitation of Meteorological Satellites
FCDR	Fundamental Climate Data Record
FMI	Finnish Meteorological Institute
FOV	Field of view
GCOS	Global Climate Observing System
GLOBE	The Global Land One-kilometer Base Elevation
GMI	GPM Microwave Imager
GPM	Global Precipitation Measurement
HOAPS	The Hamburg Ocean Atmosphere Fluxes and Parameters from Satellite data
IOP	Initial Operations Phase
KNMI	Koninklijk Nederlands Meteorologisch Instituut
MAD	Median absolute deviation
MD5	Message-Digest Algorithm 5

MSG	Meteosat Second Generation
NASA	National Aeronautics and Space Administration
NCEP	National Centers for Environmental Prediction
NDBC	National Data Buoy Center
NESDIS	National Environmental Satellite, Data, and Information System
NMHS	National Meteorological and Hydrological Services
NOAA	National Oceanic & Atmospheric Administration
NWP	Numerical Weather Prediction
PRD	Product Requirement Document
PUM	Product User Manual
QC	Quality Control
RDR	Raw Data Record
RMIB	Royal Meteorological Institute of Belgium
RMS	Root Mean Square
RSD	Robust Standard Deviation
RSS	Remote Sensing Systems
SAF	Satellite Application Facility
SI	Système international d'unités
SMHI	Swedish Meteorological and Hydrological Institute
SMMR	Scanning Multichannel Microwave Radiometer
SMMR	Scanning Multichannel Microwave Radiometer
SSM/I	Special Sensor Microwave Imager
SSMIS	Special Sensor Microwave Imager Sounder
TA	Antenna Temperature
TB	Brightness Temperature
TDR	Temperature Data Records